DEVELOPMENT OF $FeCoNi(B_xAl_{1-x})_{0.1}Si_{0.1}$ HIGH ENTROPY ALLOY (HEA) AS CATALYST FOR AZO DYE (METHYL ORANGE) DEGRADATION

BY

NUR HUDAWIYAH BINTI ABU HASSAN

INTERNATIONAL ISLAMIC UNIVERSITY MALAYSIA

OCTOBER 2023

DEVELOPMENT OF HIGH ENTROPY ALLOY (HEA) FOR AZO DYE (METHYL ORANGE) DEGRADATION

BY

NUR HUDAWIYAH BINTI ABU HASSAN

A dissertation submitted in fulfillment of the requirement for the degree of Master of Science in Engineering

Kulliyyah of Engineering
International Islamic University Malaysia

OCTOBER 2023

ABSTRACT

The Fenton process is one of the chemical oxidation degradation processes widely used in wastewater management due to being environmentally safe. It involves a reaction in which iron-catalyzed hydrogen generates a hydroxyl radical. Even though the Fenton process can degrade the azo dye (methyl orange) solution, there are still substantial limitations, such as high sludge production due to high iron and limited catalytic activity. Therefore, this study focuses on improving the azo dye (methyl orange) degradation process in the Fenton process. A novel alloy known as FeCoNi(B_xAl_{1-x}) $Si_{0.1}$ High Entropy Alloy (HEA) powders with different compositions was proposed as a catalytic material for the Fenton process. Mechanical alloying was used to produce HEA powder, which is expected to considerably improve its efficiency in the degradation of azo dye (methyl orange). The characteristics of the milled HEA powder, as well as its degradation efficiency and kinetic mechanism in the Fenton process, were investigated. FeCoNi(B_xAl_{1-x}) $_{0.1}Si_{0.1}$ (x=0.00, 0.02, 0.04, 0.06, 0.08, 0.10) powders were milled in high purity argon atmospheres for various times from 5H to 160H. The result shows milled HEA powders were diffused completely into solid solution when three phases were appeared after 160H of milling which are FCC, Fe2B and BCC/B2. The particle size reduced as the milling time increased and the particle distribution became more homogenous at 160H. The reduction of particle sizes increased the surface area, thus providing more catalytic sites for HEA. From the Fenton process, the optimum molar ratio ($[Fe^{2+}]/[H_2O_2]$) of Fenton reagents was 10:1.02. The kinetic mechanism of milled HEA powder as catalyst in the Fenton process was determined by the pseudo-first order and pseudo-second order. The highest k (decolorization rate constant) value of the HEA catalyst occurred at 30 minutes within 60 minutes of the Fenton reaction. The results showed the feasibility and efficiency of the HEA as catalytic materials in the Fenton process. Therefore, this research can contribute to the development of an appealing, low-cost, and efficient approach for HEA functional applications in wastewater management.

ملخص البحث

تعتبر عملية فينتون Fenton واحدة من عمليات تحلل الأكسدة الكيميائية المستخدمة على نطاق واسع في إدارة مياه الصرف الصحي بسبب كونها آمنة بيئيًا. أنها تنطوي على تفاعل يحفز حديد بيروكسيد الهيدروجين لتوليد جذور هيدروكسيل. على الرغم من أن عملية فنتون Fenton يمكن أن تحلل محلول صبغة الآزو azo dye (برتقالي الميثيل)، إلا أنه لا تزال هناك قيود كبيرة، مثل إنتاج الحمأة العالية بسبب وجود كمية عالية من الحديد، وأيضاً النشاط التحفيزي المحدود. ينصب تركيز هذه الدراسة على تحسين عملية تحلل صبغة الآزو (برتقالي الميثيل) في عملية فنتونFenton من خلال إنتاج مادة سبيكة جديدة تُعرف باسم مسحوق FeCoNiAlBSi High Entropy Alloy (HEA) وبمحتوى مختلف من البورون حيث تم اقتراحها كمادة محفزة في عملية فنتون Fenton. تم استخدام السبائك الميكانيكية لإنتاج مسحوق HEA، وإذ من المتوقع أن يحسن بشكل كبير كفاءته في تحلل صبغة الآزو (برتقالي الميثيل). تم فحص خصائص مسحوق HEA المطحون، وكذلك كفاءة التحلل وآلية الحركية في عملية Fenton. من نتائج XRD، ينتشر مسحوق HEA المطحونة بالكامل لتصبح HEA عند H160 من وقت الطحن. يقل حجم الجسيمات مع زيادة وقت الطحن ليصبح أكثر تجانسًا عند H160. يؤدي تقليل حجم الجسيمات إلى زيادة مساحة السطح وبالتالي توفير المزيد من المواقع التحفيزية لـ HEA. في عملية فنتون Fenton، كانت نسبة مُولِيَّة الأمثل لكواشف فنتون هي 10: 1. تم تحديد الآلية الحركية لمسحوق HEA المطحون كمحفز في عملية فنتون Fenton من خلال شبه المرتبة الأولى والمرتبة الثانية. أعلى قيمة K لمحفز HEA كانت في 30 دقيقة في غضون 60 دقيقة من تفاعل فنتون Fenton. ساهم هذا البحث في تطوير نهج رائع ومنخفض التكلفة وفعال لتطبيقات HEA الوظيفية في إدارة مياه الصرف الصحي.

Approval Page

I certify that I have supervised and read this study and that in my opinion, it conforms to acceptable standards of scholarly presentation and is fully adequate, in scope and quality, as a thesis for the degree of Master of Science in Engineering

…….

Norhuda Hidayah Binti Nordin
Supervisor

…….
Mohammed Saedi Jami
Co-Supervisor

I certify that I have read this study and that in my opinion it conforms to acceptable standards of scholarly presentation and is fully adequate, in scope and quality, as a thesis for the degree of Master of Science in Engineering

Nur Ayuni Binti Jamal
Internal Examiner

…….

External Examiner

This thesis was submitted to the Department of Manufacturing and Materials Engineering and is accepted as a fulfilment of the requirement for the degree of Master of Science in Engineering

Ahmad Zahirani bin Ahmad Azhar
Head, Department of Manufacturing
and Materials Engineering

This thesis was submitted to the Kulliyyah of Engineering and is accepted as a fulfillment of the requirement for the degree of Master of Science in Engineering

…….
Sany Izan Ihsan
Dean, Kulliyyah of Engineering

Declaration

I hereby declare that this dissertation is the result of my own investigations, except where otherwise stated. I also declare that it has not been previously or concurrently submitted as a whole for any other degrees at IIUM or other institutions.

Nur Hudawiyah Binti Abu Hassan

Signature…… Date…26/9/2023……

INTERNATIONAL ISLAMIC UNIVERSITY MALAYSIA

DECLARATION OF COPYRIGHT AND AFFIRMATION OF FAIR USE OF UNPUBLISHED RESEARCH

DEVELOPMENT OF HIGH ENTROPY ALLOY (HEA) AS CATALYST FOR AZO DYE (METHYL ORANGE) FOR AZO DYE DEGRADATION

I declare that the copyright holder of this thesis/dissertation are jointly owned by the student and IIUM.

By signing this form, I acknowledged that I have read and understand the IIUM Intellectual Property Right and Commercialization policy.

Affirmed by Nur Hudawiyah Binti Abu Hassan

…… ……26/9/2023……..

Signature Date

This thesis is dedicated to my parent for laying the foundation of what I turned out to be in life.

Acknowledgements

All glory is due to Allah, the Almighty, whose Grace and Mercies have been with me throughout the duration of my programme. Although, it has been tasking, His Mercies and Blessings on me ease the herculean task of completing this thesis.

I am most indebted to by supervisor, Assist. Prof. Ts. Dr Norhuda Hidayah binti Nordin, whose enduring disposition, kindness, promptitude, thoroughness and friendship have facilitated the successful completion of my work. I put on record and appreciate her detailed comments, useful suggestions and inspiring queries which have considerably improvedthis thesis. Her brilliant grasp of the aim and content of this work led to his insightful comments, suggestions and queries which helped me a great deal. Despite her commitments, she took time to listen and attend to me whenever requested. The moral support she extended to me is in no doubt a boost that helped in building and writing the draft of this research work. I am also grateful to my co-supervisor, Prof. Dr. Mohammed Saedi Jami whose support and cooperation contributed to the outcome of this work.

Lastly, my gratitude goes to my beloved family and lovely friends; for their prayers, understanding and endurance while away.

Once again, we glorify Allah for His endless mercy on us one of which is enabling us to successfully round off the efforts of writing this thesis. Alhamdulillah

Table of Contents

List of Tables

List of Figures

CHAPTER ONE

INTRODUCTION

1.1 Background of Study

The textile industry is one of the fastest expanding industries in Malaysia, contributing considerably to economic growth, particularly in man-made textile fibre. Malaysia produced almost 400 000 tonnes of man-made fibre, representing for around 1.03% of global production (Pang et al, 2013). Global textile production has almost quadrupled in the previous 15 years, from 2000 to 2015, due to expanding middle-class manufacturing and increased per capita sales in the developed economy (Ellen MacArthur Foundation, 2020). However, the textile industry generates 22% of Malaysia's total volume of textile industry waste water. Furthermore, the release of dyes into the environment during the textile fibre dyeing, treatment, and finishing process is responsible for approximately 20% of worldwide water pollution, according to the United Nations Environment Programme (UNEP) (2018) and the Ellen MacArthur Foundation (2020).

Dye is a colored compound that chemically binds to the substrate it is applied on. Azo dyes are colors with an azo group (N=N) in their chemical components (Gordon et al, 2012). According to Bruschweiler et al. (2017), azo dyes are the most significant category of textile dyes used in the textile industry. Additionally, azo dyes are the most widely used synthetic dye since they are inexpensive and simple to apply (Jamee et al, 2019). Because of this, azo dyes are frequently utilized in the textile sector. On the one hand, due to their toxicity and cancer-causing properties, azo dyes can harm the environment and other living organisms (Matyszczak, 2020).

Several methods, including physical adsorption, chemical treatment, chemical oxidation, and biological treatment, have been used to remove azo dye in solutions (Wu et al, 2018). The Fenton method is touted as one of these approaches' most successful methods for the degradation of a variety of hazardous and organic pollutants due to the low toxicity of the reagents utilised in it (P.V et al., 2012). The Fenton method, which employs Fe^{2+} ions to speed up the formation of the hydroxyl radical from hydrogen peroxide, is one of the advanced oxidation processes (AOPs). The pollutants are then oxidised by the reaction of hydroxyl radicals. However, the conventional Fenton process has a number of drawbacks, including a high operating cost, a narrow pH range, a huge volume of iron sludge production, and a challenging process for recycling the homogeneous catalyst, Fe^{2+} (Sabhi et al., 2001). The Electro-Fenton approach, which Matyszczak et al., (2019) claims uses the electrolysis to speed up the process and boost the efficiency of the Fenton process as the production of hydroxyl radicals will also be increased, is a good substitute to address these issues. Time and cost may be saved and decreased if this method was used to treat azo dye.

A catalyst is necessary to speed up the degradation process when treating azo dye with the Fenton method. Afterward, several different types of catalyst, including iron activated carbon (Abu Bakar et al., 2020), ferrite bismuth (Da Cruz Severo et al., 2020), two electron catalyst (Matyszczak et al., 2020), and zero valent metal (Matyszczak et al., 2019), had been found, studied, experimented with, and improved based on the conventional therapy. The catalytic activity from these studies are nevertheless sluggish and time-consuming. Therefore, it is crucial to create a new catalytic material to speed up the azo dye's degradation without creating any secondary products that call for additional processing.

A combination of five or more elements concentrations between 5% and 35% is referred to as a high entropy alloy (HEA). All elements are concentrated in HEAs, and there are no identifiable basis elements (Miracle et al, 2019). Few compositions of HEAs powder such as AlCoCrFeNi, CoCrFeMnNi, AlFeMnTiCr, AlFeMnTiCo and AlFeMnTiNi have been studied in degrading dye in solution (Wu et al., 2019 & Lv et al., 2016). According to Wu et al., (2019) and Lv et al., (2016) due to HEAs powder highly complex atomic structure with severe lattice distortion, chemical composition effect, residual stress and high specific surface area, HEAs can enhance the degradation process of dye. Besides, Lv et al., (2016) stated the reduction of azo dyes corresponds to their degradation. In their studies proved that HEA was stronger reducing agents with higher constituent reactivity result in degrading azo bond "-N=N-" into two "-NH_2" molecules. These factors make HEAs more capable of modifying adsorption qualities and give them a higher potential energy, which allows them to produce more catalytic active sites (Cui et al, 2018). High entropy alloys (HEAs) are suggested here as a catalytic material to improve Fenton's process efficiency. There have only been a few literary studies conducted by the researchers, and the catalytic reaction and properties of the HEA as a catalyst in degradation azo dye have not yet received much attention. The majority of HEA's studies concentrate on structural and refractory applications due to its exceptional hardness, strength, and capacity to withstand high temperatures (Tsai et al., 2014).

1.2 Problem Statement

Wastewater is frequently treated using the Fenton method. This technique concentrates on organic pollutants since they can be oxidised by the hydroxyl radical to produce water and oxygen. The disadvantages of the process include its high operating

costs, large volume of sludge produced, difficulty recycling the homogeneous catalyst ([Fe^{2+}), and a narrow pH range where it always performs best (pH 3). This is because as pH rises, [Fe^{3+} hydrolysis and precipitation in the solution can decrease the reaction's catalytic capacity (Wang et al, 2015). The vast amount of sludge produced by this approach makes recycling it difficult and necessitates labor-intensive purification, therefore operational costs are significant.

$FeCoNi(B_xAl_{1-x})_{0.1}Si_{0.}$ HEAs, a unique class of multicomponent alloys, may replace iron salt in the Fenton reaction due to HEA excellent catalytic properties. Although HEA catalytic characteristics have not been investigated, it was previously believed that the stability of solid solutions (SS) made HEAs unstable which resulting in excellent catalytic properties of HEA (Wu et al., 2016 & Lv et al., 2016). According to research, alloying additives and synthesis processes can modify the intermetallic and SS phases of HEA. Due to the intricacy of its surface, HEA will also act as a catalyst in the Fenton reaction by exchanging ferrous ions. The bigger active site of HEAs may lead to a greater production of oxidising agents during the Fenton reaction and stronger reducing agents in degrading azo bond.

Additionally, there are just a few literary studies that the researchers have explored on HEA's catalytic capabilities in degrading azo dye in solution. Understanding the kinetic reaction of HEA is crucial because HEA can behave differently as a catalyst and HEA catalyst reaction is yet unknown and unexplored.

1.3 Research Objectives

1. To develop and characterize $FeCoNi(B_xAl_{1-x})_{0.1}Si_{0.}$ HEAs powder as catalyst by mechanical alloying.
2. To optimize the performance of $FeCoNi(B_xAl_{1-x})_{0.1}Si_{0.1}$ HEAs powder as catalyst in Fenton process for degrading azo dye (methyl orange)
3. To study kinetic reaction of $FeCoNi(B_xAl_{1-x})_{0.1}Si_{0.}$ HEAs as a catalyst in Fenton process

1.4 Significant of Study

The significance of this study is to explore a new catalytic material for degrading azo dye (methyl orange) in order to save the environment and to establish one of the Sustainable Development Goals (SDGs) which is clean water and sanitation. Firstly, HEA is the new catalytic material that is able to give superior properties and excellent efficiency. The chief importance of this learning is to evaluate the efficiency of HEA powder as a catalyst in azo dye (methyl orange) degradation. The problem regarding wastewater of azo dye (methyl orange) becomes a major contribution to environmental pollution and causes damage. Even though there are methods and catalysts that are already used in order to remove the azo dye (methyl orange) from the water, there are some disadvantages that may limit the process and catalytic activity. Hence, this study on HEA will help to improve the properties of catalytic materials. Secondly, study on development of high entropy alloys (HEAs) may open a solution to save the environment from wastewater pollution and carcinogenic effects on humans. This is because, river is the main source of water for plants and humans and if it is not treated well before being released it may damage the ecosystem

and become the cause of dangerous diseases such as cancer. Besides that, the main idea of this study is also to establish one of the Sustainable Development Goals (SDGs) which is clean water and sanitation. Thus, the research on HEA as new catalytic materials is necessary to broaden the choice of solution to solve problem that occurs now or in the future.

CHAPTER TWO

LITERATURE REVIEW

2.1 Azo Dye

Untreated textile effluent has high levels of colour, chemical oxygen demand (COD), biochemical oxygen demand (BOD), total organic carbon (TOC), suspended solids (SS), pH, temperature, turbidity, and toxicity. This is because colours are released into the environment during the dyeing and finishing of textile fibres. Pang et al. (2013) estimate that 90% of dyes are utilised in the textile industry, with the remaining 10% used in the leather, paper, plastic, and chemical sectors. Dyes are coloured compounds that chemically bond to the substrate on which they are applied. Dyes are divided into two groups based on their function: chromophores and auxo-chromes. As shown in Figure 2.1, the functional groups of chromophores are delocalized systems with conjugated double bonds that are generally electron withdrawing groups such as -C=C-, -C=N-, -C=O-, -N=N-, -N=O-, and -NO-, whereas auxo-chromes are electron donating substituents such as -NH-. Acid, reactive, basic, vat, and sulphur dyes are the different types of dyes in the colour index. Azo dye (specified by the symbol -N=N-) account for 65-70 percent of total dye synthesis in these groupings. According to the Ecological and Toxicological Association of the Dyestuffs Manufacturing Industry (ETAD) (Pang et al., 2013), basic dye and diazo direct dyes had the greatest toxicity among 4000 dyes studied. Azo dye has a high colour intensity, a medium colour fastness, are cheap, and are insoluble in water. Azo dye is widely used in the textile sector because of their low cost. Furthermore, azo dye is insoluble in water,

resulting in water pollution that can affect individuals and the environment owing to their toxicity and carcinogenicity.

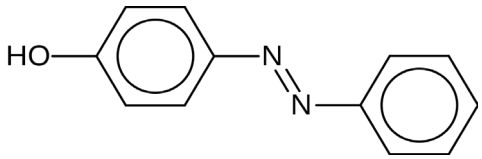

Figure 2.1 Chemical Structure of Azo dye (Ragimiri, 2006)

2.2 Azo Dye Degradation Method

It is apparent that textile dyes must be degraded from wastewater properly. Hence, various methods have been proposed to treat the textile dye effluents economically and efficiently. The methods are categorized into three groups consisting of physical, biological, and chemical and chemical oxidation treatment processes as shown in Table 2.1. The application of these approaches depends on the type of wastewater treated and the cost-effectiveness of treatments.

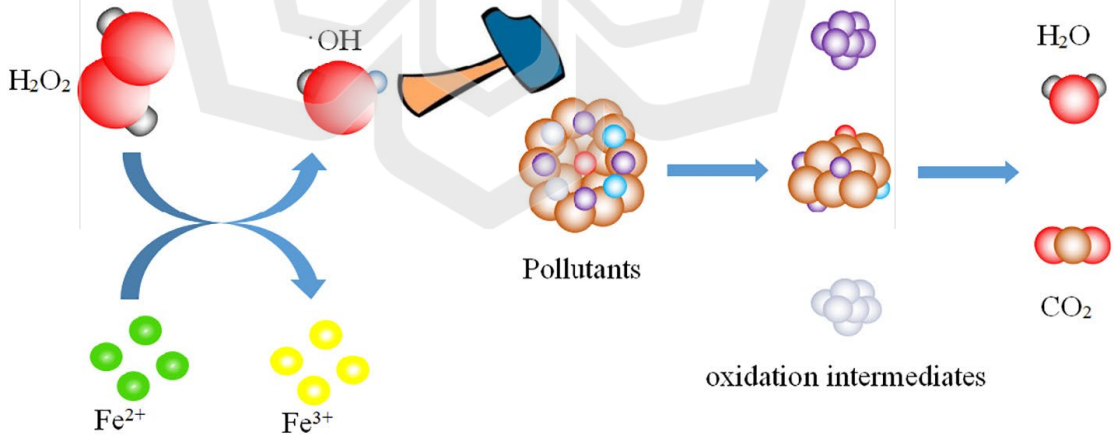

Figure 2.2 Fenton process mechanism (Zhang et al., 2019)

Table 2.1 Current available technology for dye treatment (Pang et al., 2013)

TREATMENTS METHODS	TYPES	ADVANTAGES	DRAWBACKS
Physical Treatment	Adsorption	• Effective dye removal for a variety of colours	• Need a disposable or regenerable adsorbent
	Ion Exchange	• No adsorbent was lost during regeneration	• Ineffective for all dyes
	Membrane Filtration	• Effective dye removal for all types dye	• Production of concentrated sludge, high operating costs, and inability to handle big volumes
Biological Treatment	Aerobic process	• Effective azo dye removal • Reduced operational costs; and recyclable sludge	• Greater land requirements, longer detention periods, and vulnerability to harmful organic dye

	Anaerobic process	• Lower running costs and the ability to use the biogas produced as a fuel source	• Greater sensitivity to hazardous organic dye, a longer time for the cell to replicate, and the synthesis of aromatic amine
Chemical Treatment	Chemical Coagulation and Flocculation	• For different types of dyes, short detention times and high removal efficiencies	• pH adjustments and chemical reagents are very expensive. • Sludge production issues, handling issues, and disposal issues
Chemical oxidation	Fenton oxidation	• Rapid and efficient removal of a variety of dyes	• Issues with handling and disposal, excessive sludge production, and expensive chemical reagent costs
	Ozonation	• Effective dye removal for a variety of colours	• Not practical for dispersion dyes.

		• No sludge production	
	Photocatalytic and sonocatalytic oxidation	• Effective dye removal for a variety of colours	• Newly developed techniques. emergence of a byproduct. However, compared to ultrasonic irradiation, UV light is frequently less permeable in aqueous media.
	Radiolysis	• Mineralization was completed in a short period of time. • No sludge production • Effective dye removal for a variety of colours.	• Only suitable for dyes with a higher concentration • Comparatively new approach

2.3 Fenton Process

On the basis of the conventional treatments, as shown in Table 2.1, a number of dye treatments have been identified, investigated, tested, and improved. The Fenton process is one of the well-known and often performed. In 1894, H.J.H. Fenton presented a study on the interaction of ferrous ions, Fe^{2+} with various oxidising agents, which led to the discovery of the Fenton reagent. One of the advanced oxidation processes (AOP) is the Fenton process, which uses ions to catalyse the production of hydroxyl radical from hydrogen peroxide. Then, as depicted in Figure 2.2, hydroxyl radicals react and oxidise the contaminants. Advanced oxidation techniques (AOP) have been successfully used to eliminate persistent organic contaminants (Raman et al., 2019). Fenton reagent is used to oxidise harmful substances, remove colour, and inactivate germs and viruses. The Fenton process can be used to degrade azo dye in solution. Elodie Guivarch et al. (2003) demonstrate that the Fenton process can breakdown azo bonds along with their substituent, primarily benzene and naphthalene derivatives. Chen et al. (2001) further demonstrate that the disappearance of the phenyl group's characteristic infrared (IR) peak following interaction with OH indicates the formation of carboxylic intermediates. Elodie Guivarch et al. (2003) developed a general reaction mechanism for mineralization of azo dye molecules by the oxidative action of hydroxyl radicals in the Fenton to prevent the production of hazardous byproducts during the degradation process as shown in Figure 2.3. The Fenton process is then a practical way to lessen the toxicological effects of the azo dye's vibrant colors.

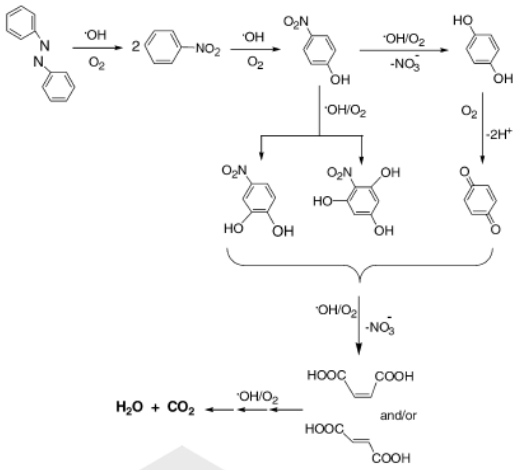

Figure 2.3 Mineralization pathway during Fenton process (Elodie Guivarch et al., 2003)

2.3.1 Conventional Fenton

Homogeneous and heterogeneous Fenton reactions are the two subtypes of the conventional Fenton process. The conventional Fenton reaction, known as homogeneous Fenton, consists of three phases in processing. As depicted in Figure 2.3, the catalyst dissolves first, then an OH radical is produced, and finally, organic materials are oxidized. Fenton reaction does not provide good efficacy in neutral pH circumstances because Fenton reaction is mostly dependent on the degree of iron catalyst dissolution. The aqueous medium must change to an acidic state, which favors the catalyst's dissolution, in order to improve the reaction. Nearly all researchers came to the conclusion that the ideal Fenton reaction conditions are in an acidic environment with a pH of 3. (Sajid Hussain et al., 2021). The Fenton reagents were changed via the heterogeneous Fenton reaction from $Fe^{2+}$to Fe^{3+} or other transition metal ions. As shown in Figure 2.4, the heterogeneous Fenton reaction has three reactions: adsorption of organics on the catalyst surface, production of OH radicals at the catalyst surface's active sites, and oxidation of the organics followed by

desorption of the oxidation products from the catalyst surface. Although heterogeneous Fenton similar reactions coexist with homogeneous Fenton reactions, as shown in Figure 2.5, they can be employed to minimize some of the drawbacks of the latter, including strong chemical input, a strong acid environment, and high sludge output (Yuan et al., 2013).

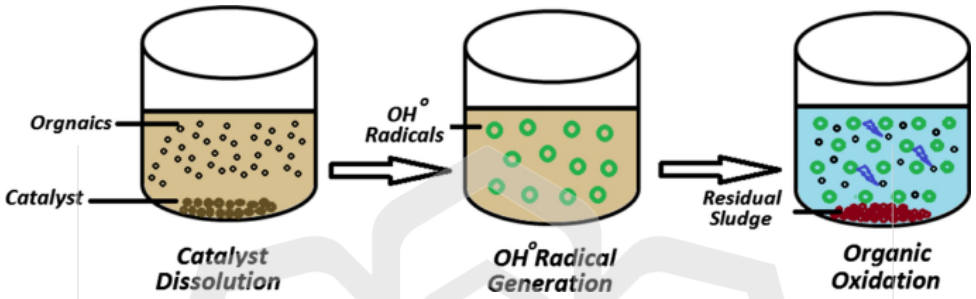

Figure 2.4 Homogeneous Fenton process (Sajid Hussai et al., 2021)

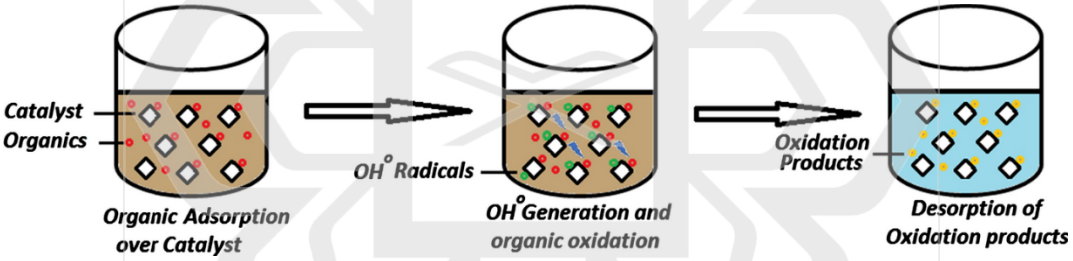

Figure 2.5 Heterogeneous Fenton process (Sajid Hussai et al., 2021)

Furthermore, in order to counteract these benefits, researchers focused mainly on improving the Fenton process. Ferric oxide, iron minerals, and nano-zero valent iron were utilised as catalysts to substitute Fe^{2+} in both homogeneous and heterogeneous processes (Xu et al., 2020). On the one hand, the use of redundant or transition metals can minimise iron loss and sludge generation, giving birth to the heterogeneous Fenton process. Accordingly, some external energy is added into the Fenton process to increase hydroxyl radical synthesis while decreasing sludge production, such as the electro-Fenton method

(Alfaya et al., 2015), sono-Fenton like process (Wang et al., 2015) and photo-Fenton like process (Dehghani et al., 2014). These Fenton-like processes known as phenomenon assisted Fenton-like processes (Wang et al., 2016).

2.3.2 Electro Fenton Like Process

Electro Fenton process is the combination process of electrochemical process and Fenton-like process during wastewater treatment to improve Fenton-like process. Fe^{2+} and H_2O_2 were produced by the electrochemical method as Fenton reagents. For the electro-Fenton process, the catalyst and source of oxidant depends on the heterogeneous and homogeneous Fenton like-process, hence it is very diverse. In which, H_2O_2 is generated in situ via a reduction of dissolved oxygen on the surface of the cathode in an acidic solution. Homogenous metal catalysts are placed as sacrificial anodes in the electrochemical cells and the metal catalyst will be regenerated on the surface of the cathode. Examples of metal catalysts, M^{n+}: Fe^{2+}, Mn^{2+}, Cu^{2+}, and Co^{2+}. This shows that the Fenton process is being applied in the electrochemical process. Reactions that occur in the electrochemical process include (Matyszczak et al., 2019):

$$O_2 + 2H^+ + 2e^- \rightarrow H_2O_2 \text{ (Equation. 2.1)}$$

$$M^{(n+1)+} + e^- \rightarrow M^{n+} \text{ (Equation. 2.2)}$$

This is an advantage to the Fenton process as this increases the efficiency of organic degradation, decreases the cost process, and reduces the cost of transportation. This Fenton-like process has been widely studied and used to degrade organic pollutants such as dyes, pesticides, amines, and phenolic compounds. Moreover, this process is relatively simple

and cheaper as it does not require reactors. Figure 2.6 shows typical electro-Fenton-like systems.

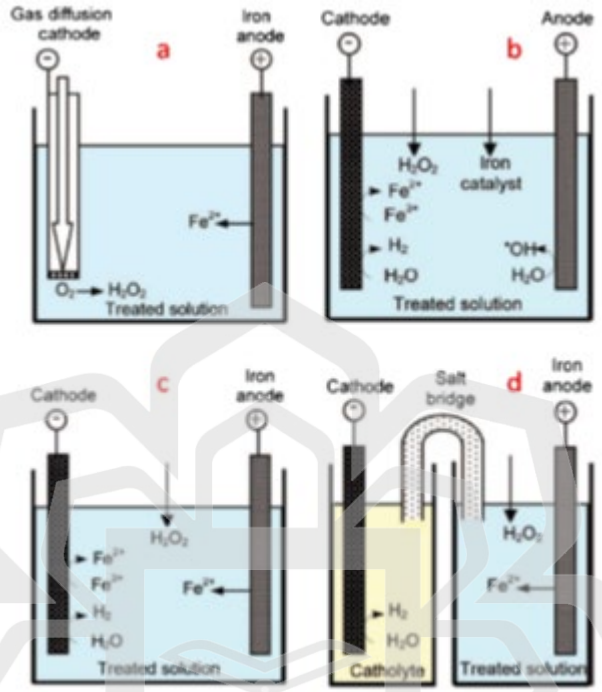

Figure 2.6 Typical electro-Fenton-like systems (Wang et al., 2016) a) Peroxi-coagulation (PC) process b) EF-Fere process c) Electrochemical peroxidation (ECP) process d) Anodic Fenton (AFT) process

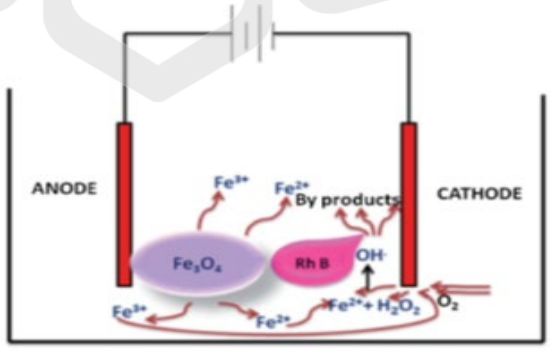

Figure 2.7 Degradation mechanism of dye in magnetite-catalysed Fenton-like process (Nidheesh et al., 2014)

As shown above, the researchers have made several changes to the Fenton-like processes in order to observe the increase or decrease in efficiency of the wastewater treatment. In summary, electro-Fenton process is a second generation Fenton process, in which the continuous electro-generation of H_2O_2 from cathode reduction of O_2 combined with the supply of Fe^{2+} continuously regenerated on the cathode can allow for the formation of •OH. The advantages of electro-Fenton process compared with conventional Fenton process are as follows: (1) the on-site production of H_2O_2, which can avoid the risks related to its transport, storage, and handling; (2) the continuous regeneration of Fe^{2+} on the cathode, which can minimize the iron sludge production and improve the degradation efficiency of organic pollutants. However, electro-Fenton process should be improved by overcoming its disadvantages such as low H_2O_2 yield, low cell voltage, low current density and low conductivity (Martínez-Huitle and Brillas, 2009; Yuan et al., 2011; Sirés et al., 2014).

2.3.3 Photo-Fenton Like Process

In both heterogeneous and homogeneous Fenton-like reactions, the purpose of photochemistry is to provide energy utilising ultraviolet and/or visible light to reduce the catalyst loading and/or to increase the catalytic capacity of the catalyst; the essence is connected to the redox processes (HD et al., 2002). Researchers have accepted the photo-induced reductive breakdown of the solid catalyst in the heterogeneous photocatalytic system. As Fe^{3+} oxide has been the subject of extensive research, iron oxide is used in this review as an example to demonstrate the suggested mechanism. Figure 2.8 depicts the hypothesised scenario for the photo reductive dissolution of -FeOOH (HD et al., 2002).

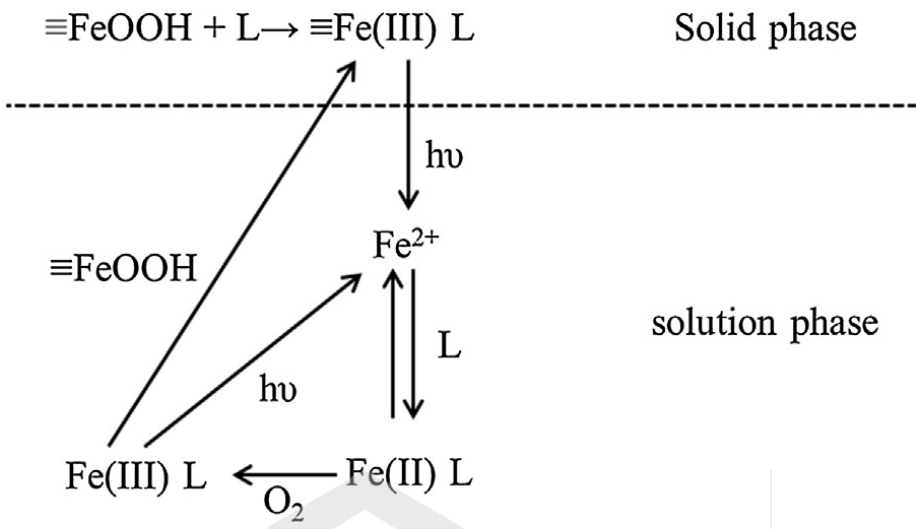

Figure 2.8 Mechanism of Fe (III) (HD et al., 2002)

In homogeneous photo-Fenton-like systems, the photochemical reduction of the metal catalyst is the main pathway throughout the catalytic oxidation process. Two additional processes can take place as a result of light irradiation in the photo- Fe^{2+} -H_2O_2 system, in addition to the reactions in the Fe^{2+} and H_2O_2 system. Equation 2.3 describes how Fe^{3+} ions, which are present in acidic environments as $Fe(OH)^{2+}$ undergo a photochemical reduction process to yield Fe^{2+} ions. In the second reaction, Fe^{2+} and H_2O_2 produces OH^- by a photolysis process under shorter wavelength radiation (equation 2.4). (2002) (HD et al.).

$$Fe(OH)^{2+} \rightarrow Fe^{2+} + OH^- \text{ (Equation 2.3)}$$

$$H_2O_2 \rightarrow 2OH^- \text{ (Equation 2.4)}$$

Photo-generated ferrous ions (equation 2.3) can enter the Fenton system directly, producing additional HO and thus improving the organic pollutant removal rate. In summary, the photo-Fenton system uses the energy provided by ultraviolet or visible light

to accelerate the reduction of Fe^{2+} to Fe^{3+} which can reduce iron sludge production and the initial Fe^{2+} concentration input, as well as improve the photo-Fenton system's oxidation ability and organic pollutant degradation efficiency. However, the photo-Fenton process has significant drawbacks, such as low light energy consumption, high operation costs, and photo-reactor design, which restrict the development of the photo-Fenton process on a wide scale (Pérez et al., 2013; Pliego et al., 2015; Wang et al., 2016).

2.3.4 Heterogeneous Catalyst Used in Fenton Process to Degrade Azo Dye

A catalyst is required to enhance the Fenton reaction in order to degrade azo dye. The degradation of azo dye (methyl orange) in the Fenton process can then be accelerated by replacing the conventional catalyst, Fe^{3+} with more advanced catalysts such as Fe-Ac, two electron catalyst, ferrite bismuth ($BiFeO_3$) catalysts generated by hydrothermal technique EDTA, and other metal catalysts, as indicated in Table 2.2. This is known as a heterogeneous Fenton-like reaction.

However, compared to other catalysts in different articles and studies as shown in Table 2.2 and Table 2.3, high entropy alloys (HEAs) have a higher degradation rate which is 11 minutes to degrade azo dye completely. On the other hand, there is still no further study on high entropy alloys (HEAs) as a catalyst in the Fenton process. Thus, this study will focus on catalytic activity of HEAs as a catalyst in the Fenton process to degrade azo dye for wastewater management.

Table 2.2 Catalyst used in Fenton process to remove azo dye

AUTHOR	TITLE	KEY FINDINGS	ADVANTAGES	DRAWBACKS
Abu Bakar Muhamad, Ahmed Lawal Mashi (August, 2020)	Application of Central Composite Design to the Photo Fenton Degradation of Methyl Orange Azo dye (methyl orange) Using Fe-Activated Carbon Catalyst	● This research is focused on utilization of Fe^{2+} catalyst loaded activated carbon (Fe-ac) and H_2O_2 (aqueous) in a Photo-Fenton's process to generate hydroxyl radicals that mineralize methyl orange dyes. ● Compared Photo-Fenton's method with conventional Fenton's method and adsorption method with the presence of Fe-ac as catalyst to degrade methyl orange (azo dye ● Focus on finding the optimization of catalyst dosage (Fe-ac), pH, amount	● Photo-Fenton's process can remove methyl orange dye up to 75% compared to conventional Fenton's process (44%) and adsorption method (12.5%)	● Doesn't include the detailed mechanism of the catalyst to remove methyl orange in the Fenton's process ● Do not determine the total dissolved solid after remove the methyl orange

		of H_2O_2 , methyl orange concentration and time taken to degrade methyl orange		
Da Cruz Severo, Eric; Dotto, Guilherme Luiz; Silvestri, Siara; dos Santos Nunes, Isaac; Silveira Salla, Julia; Martinez Cruz, Azael; Boit	Improved catalytic activity of EDTA–modified BiFeO3 powders for remarkable degradation of procion red by heterogeneous	● Heterogeneous photo–Fenton degradation of Procion Red dye under visible irradiation was investigated using ferrite bismuth (BiFeO3) catalysts synthesized by hydrothermal method with and without EDTA. ● BiFeO3 catalyst was successfully synthesized by a simple hydrothermal method.	● Reaching 99% of degradation in 120 min with the presence of (BiFeO3) catalysts synthesized by hydrothermal method with EDTA ● Catalyst showed outstanding	● Do not determine the total dissolved solid after Procion Red degradation

Martinello, Katia; Foletto, Edson Luiz (2020)	photo–Fenton process		decolorization efficiency of dye after five cycles	
Matyszczak, Grzegorz; Krzyczkowska, Katarzyna; Fidler, Aleksandra (2020)	A novel, two-electron catalysts for the electro-Fenton process	• Substituting Fe^{2+} catalyst with Sn^{2+} and Bi^{3+} (two electron catalyst) as catalyst in Fenton's process • Compare degradation efficiency of Metanil Yellow and triarylmethane dye Bromocresol Green between conventional catalyst, Fe^{2+} and two electron catalyst, Sn^{2+} and Bi^{3+} catalyst in Fenton's process in 80 min long reaction	• Two electron catalyst enhance the performance of Fenton's process in degrading Metanil Yellow: $Bi^{3+} - 56.15\%$ $Sn^{2+} - 56.63\%$ $Fe^{2+} - 51.63\%$	• Decrease the performance of the electro-Fenton process in the degradation of model triarylmethane dye Bromocresol Green in 80 min long reaction: $Bi^{3+} - 72.61\%$

				$Sn^{2+} - 63.02\%$ $Fe^{2+} - 82.67\%$ ● Do not determine the total dissolved solid
Matyszczak, Grzegorz; Sędkowska, Agata; Kuś, Stanisław (2019)	Comparative degradation of Metanil Yellow in the electro-Fenton process with different catalysts: A simplified kinetic model study	● Different catalysts have been used: Fe^{2+}, Co^{2+}, Mn^{2+}, Ni^{2+}, and Ce^{3+} to compare their catalytic activity in the electro- Fenton process.	● Did both experimental and kinetic model simulation to observe the activity of the catalyst in the Fenton's process. ● It is possible to enhance the degradation	● Doesn't include the detailed mechanism of degradation of a molecule of dye. ● Do not determine the total dissolved solid after remove the Metanil Yellow for each catalyst

			efficiency of classical electro-Fenton reaction by substituting Fe^{2+} catalyst cations with Co^{2+} Ni^{2+} and even Mn^{2+} cations	● It was found that Ce^{3+} catalyst cations decrease the performance of the electro-Fenton process.

2.4 Decolorization Kinetics Studies of Fenton Reaction

A kinetic study has been performed in the Fenton reaction based on the experimental data by using classical models such as zero-, pseudo first order and pseudo second order models, and BMG which has been developed by Chan and Chu (2003) and Behnajady et al. (2007), respectively, to determine the compatibility the Fenton experimental data with the kinetics models (Gökçe, 2022). Linearized equations of these kinetic models are:

$$C_t = C_0 - k_0 . t \quad \text{(Equation 2.5)}$$

$$\ln C_t = \ln C_0 - k_1 . t \quad \text{(Equation 2.6)}$$

$$1\, C_t = 1 C_0 - k_2 . t \quad \text{(Equation 2.7)}$$

$$t[1 - (C_t\, C_0)] = m + b . t \quad \text{(Equation 2.8)}$$

where $k_0 k_1$ and k_2 are the apparent kinetic rate constants of zero-order, 1 st-order, and 2nd-order pseudo models, respectively. For BMG model, m and b are the two constants obtained; their inverses corresponding to initial reaction rate (1/m) and maximum decolorization capacity (1/b) (Chan et al., 2003 & Behnajady et al., 2007). However according to Giwa et al., (2019), the absorbance of the detected compound is proportional to its concentration according to the Lambert-Beer equation and as such the absorbance can be used in the rate expression instead of concentration.

Pseudo first order kinetic: $\ln \frac{Ao}{At} = -kdt$ (Equation 2.9)

Pseudo second order: $\frac{t}{A_t} = \frac{1}{k_2 A_e^2} + \frac{t}{A_e}$ (Equation 3.0)

Based on the previous studies, the persistence of the negative value for k_2 indicates that the pseudo-second order kinetic model was unable to satisfactorily explain the experimental

results. The inclusion of just one reactant theoretically establishes a reaction's pseudo-first order, whereas the involvement of both reactants theoretically establishes a reaction's pseudo-second order. Pseudo first order and pseudo second order model has been applied in different studies to describe the dye removal kinetics with the Fenton process (Giwa et al., 2019; Nicodemos et al., 2022 & Gokce et al., 2023).

2.5 High Entropy Alloys (HEAs) As Catalyst

Two fundamental theories that were created by two distinct research teams for two distinct goals and published in 2004 led to the development of high entropy alloys (HEAs). The unexplored middle regions of the multi-element phase diagram, where all alloy elements are concentrated but no obvious base elements are present, are the focus of both theories. High entropy alloys (HEAs) are described as single phase solid solutions comprising at least five primary elements, each with an atomic concentration ranging from 5% to 35%, in contrast to normal alloys, which frequently only contain one, two, or three elements (Yeh et al., 2004). The main benefit of HEAs over conventional alloys is the maximization of configurational entropy, which increases the system's stability and gives it remarkable physicochemical and mechanical features like promising resistance to wear, oxidation, and corrosion as well as remarkable thermal strength.

The name "high entropy alloys" comes from the fact that their liquid or random solid solution states have significantly higher mixing entropies than conventional alloys. This implies that multi-element alloys could produce a plethora of phases and intermetallic compounds with high stability systems. In contrast to conventional alloys, the alloys tend to form simple phases with nano-crystalline and even amorphous structures (Tsai, 2014). Mixing produces structures consisting of a mixture of simple solid solutions (face-centered-

cubic (FCC), body-centered-cubic (BCC), or hexagonal close packing (HCP) due to the HEA's high configurational entropy (Yu et al., 2013).

HEAs are multicomponent alloys with a well-ordered crystal structure and randomly distributed constituent elements that have a lot of potential for fine-tuning adsorption properties. Their inherent surface complexity may provide a near-continuum distribution of adsorption energies at surface sites while increasing the fraction of optimal active sites (Yang et al, 2014). Furthermore, because HEA's atomic structure is highly complex, with random element occupancies in the lattice, its crystal structure can be highly distorted with the addition of non-negligible residual strain. Due to the various atomic sizes of each component, the HEA lattice is typically severely distorted (Qiu et al., 2019). Hence, the atoms in the HEA being in a thermodynamically metastable condition, giving them a larger potential energy and more catalytic active sites (Cui et al, 2018). Additionally, a significant lattice distortion or crystal flaw increases catalytic activity. Noble metal-based HEAs and non-noble metal-based HEAs can be used as catalysts, respectively. Ag, Au, Pd, Pt, Rh, Ru, and Ir are among the noble metals in the first group, whereas Co, Ni, Fe, Mn, Cr, Mo, and Al are among the transition metals in the second group (Gracita et al., 2012). Importantly, non-noble HEAs have been touted as affordable replacement catalysts that could reduce the need for noble metals.

2.6 Degradation Performance of HEAs Towards Azo Dye

Few studies have been done on degradation performance of High Entropy Alloys (HEAs) toward azo dye. L. Ji et al. (2020) synthesized Fe78Si13B9 amorphous alloy ribbons and high-entropy amorphous alloy ribbons of (FeCoNi)78Si13B9 by melt spinning method while Wu et al. (2019) and Lv et al. (2016) synthesized AlFeMnTiM (M = Cr, Co,

Ni) powder respectively by mechanical alloying method to determine the performance of HEAs in degrading azo dye However, HEAs in powder state have higher degradation rate compared to bulk HEAs due to high specific surface areas with more active sites exposed, which would enhance the metal utilization efficiency and catalytic activities as shown in Table 2.3 (Li et al., 2020).

Table 2.3 Degradation performance of HEAs in degrading azo dye (Li et al., 2020)

HEAS	**STATE**	**DEGRADATION RATE / MIN**	**REFERENCE**
FeCoNiSiB	Bulk/Ingot	70	L.Ji. et al. (2020)
AlFeMnTiM (M=Cr, Co, Ni)	Powder	AlFeMnTiCr = 11 AlFeMnTiCr = 22 AlFeMnTiNi = 30	Wu et al. (2019)
AlCoCrTiZn	Powder	15	Lv et al. (2016)

According to Shi Kai Wu et al. (2019), the superior degrading performance of HEAs is due to three major causes. First, due to particular alloy components and severe lattice distortion of the HEAs crystal structure, the surface of HEAs powder is electrochemically inhomogeneous, resulting in the development of a significant number of nano-galvanic cells among the elements. A nano-galvanic cell is made up of two separate components and a dye solution, and a huge amount of nano-galvanic occupy the surface of HEAs. The active metals serve as anodes, receiving electrons and catalysing azo dye molecules to produce hydrogen ions and electrons. After the dye molecules mix with hydrogen ions and electrons,

the azo bonds are broken. The process is shown in the following formula (Shi Kai Wu et al., 2019):

$$M \rightarrow M^{+} + ne^{-} \text{ (Equation 3.1)}$$

$$H_2O \rightarrow H^{+} + OH^{-} \text{ (Equation 3.2)}$$

$$R - N = N - R_1 \ + 4H^{+} + 4e^{-} \rightarrow \ R - NH_2 + R_1 - \ NH_2 \text{ (Equation 3.2)}$$

The possible degradation and mineralization process of azo dye by HEAs can be seen from Figure 2.7. Second, the combination of unique crystal structure with severe lattice distortion, residual stress and stored plastic deformation energy of HEAs possess more potential energy and active sites which are responsible for excellent degradation capacity of HEAs powder toward an azo dye. Third, the reduction behavior of nascent hydrogen ([H]) plays a role as a reduction agent to reduce various organic species. The [H] can induce the cleavage of azo bonds and destroy the chromophore groups because [H] exhibits high reactivity. The nascent hydrogen ([H]) is formed when a large number of electrons are released by HEAs and combine with hydrogen ions in water. Thus, HEAs as catalyst in Fenton process will enhance the degradation performance of azo dye by release a large number of electron and increase the formation hydroxyl radical during the Fenton process in order to break the azo bond and decolorized the azo dye effluents.

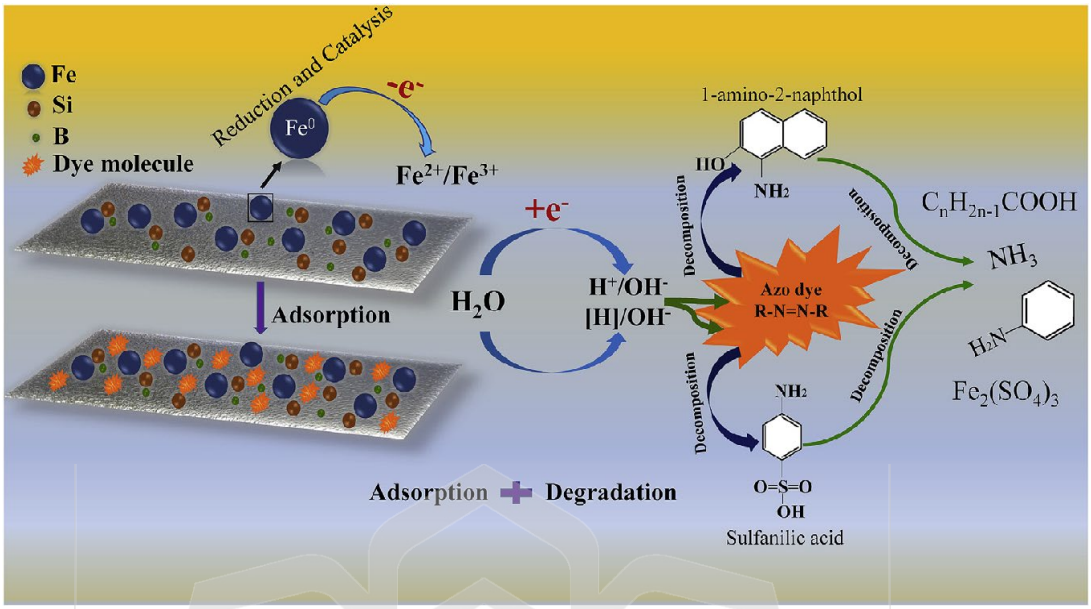

Figure 2.9 Possible degradation and mineralization of HEA (Lv et al., 2016)

2.7 Catalytic Performance of High Entropy Alloy (HEA)

2.7.1 Catalytic Mechanism of HEAs by Computational Method

Computational method has provided the means for better understanding in the catalytic process since it will give direct results on adsorption energy of molecules and intermediates on the surface of the heterogeneous catalyst which both of these are good descriptors for catalytic activity. Thomas et al. (2019) introduced a methodology for calculating adsorption energies on a complex alloy specifically for HEAs. Thomas et al. (2019) used the Density Functional Theory (DFT) model in finding the adsorption energies of RuIrRhPtPd HEAs as a catalyst in oxidation reduction reaction (ORR). The OH· and O adsorbates from the ORR were placed on top and FCC hollow binding sites, shown in Figure 2.8, respectively and the adsorption energies calculated with DFT. Then, from Figure 2.9, specific binding sites with the maximum adsorption energy can be determined.

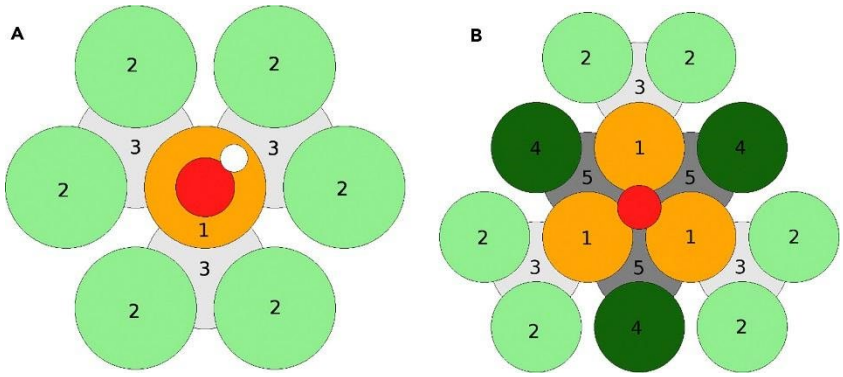

Figure 2.10 Surface configuration of HEAs (Thomas A.A et al., 2021)

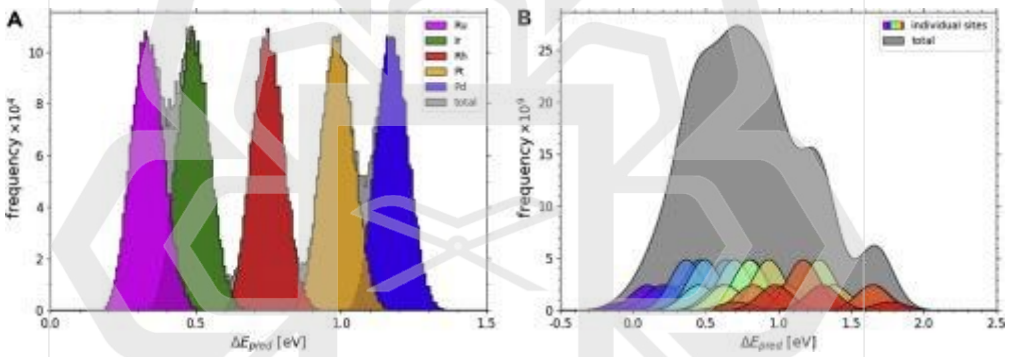

Figure 2.11 Full span of predicted adsorption energies (Thomas A.A et al., 2021)

Then, the results from the DFT model will be supported with Sabatier volcano equation to determine catalytic activity of HEAs (Thomas A.A et al. 2021) :

$$A = \sum_{I=1}^{Z}\left(\prod_{k}^{metals} f_{k}^{n_{ik}}\right) \exp\left(-\frac{|\Delta E_i - \Delta E_{opt}|}{k_B T}\right) \quad \text{(Eqn. 2.8)}$$

Where,

$Z =$ total number surface of configurations

$f_k =$ the atomic fraction of element k

$n_{ik} =$ number of element k in the surface configuration i

$\Delta E_i =$ modeled adsorption energy for the ith surface configuration,

E_{opt} = optimum adsorption energy according to Sabatier principle

k_b = Boltzman constant

T = absolute temperature

The surface of an HEA provides a near-continuum of adsorption energies because of the many surface configurations, and the full set of adsorption energies can be spanned out as predicted by a simple model. The computational simulation of HEA catalytic activity provides an accurate and time-efficient mapping between adsorption energy and surface structure that is crucial for the success of the optimization.

2.8 **SUMMARY**

Most of the literature reviews the development of high entropy alloy for structural applications that focuses on the mechanical properties of the HEA. Only recently, the studies of HEA have been expanded to functional applications such as magnetic and electrical properties. Besides, literature also merely highlighted on the utilization of alloy as catalyst especially in Fenton process. Conventionally, the literature only focused on the treatment method with limited study on the catalytic function to improve the Fenton process. Therefore, the introduction of multicomponent element alloys as the catalyst in degradation of azo dye (methyl orange) in Fenton process yet be explored in details. It was found that the catalytic properties of HEAs in degradation of azo dye (methyl orange) in the Fenton process is yet to be explored in detail. Besides, there is no further and detailed study on the kinetics reactions of High Entropy Alloys (HEAs) as a catalyst in Fenton's process where it will be explored and discovered in this study by using Arhenius equation.

CHAPTER THREE

METHODOLOGY

3.1 Methodology Flow Chart

This chapter emphasizes the experimental techniques namely sample preparation, characterizations testing and analytical techniques in the research project. The experimental set-up for the research also is discussed in this chapter. The flowchart is shown in Figure 3.1. This research consists of two phases; the first phase involves the development of HEA powders with different boron content. This was conducted by doing optimization of milling time. The synthesized $FeCoNi(B_xAl_{1-x})_{0.1}Si_{0.1}$, where x= 0, 0.02, 0.04, 0.06, 0.08, 0.1. HEA powder then was characterized to determine the crystal structure, phase morphology, elemental analysis and particle sizes using XRD, SEM, FESEM, EDS, CHNS and Particle Analysis Zetasizer machine respectively. In the second phase, the developed HEAs powder was applied as a catalyst in Fenton's process to degrade azo dye (methyl orange). The effect of adding HEAs as a catalyst in the Fenton process was observed and characterized through visual observation, UV-Vis. Next, the kinetic reaction of the alloy catalyst is was analyzed using Arrhenius equation.

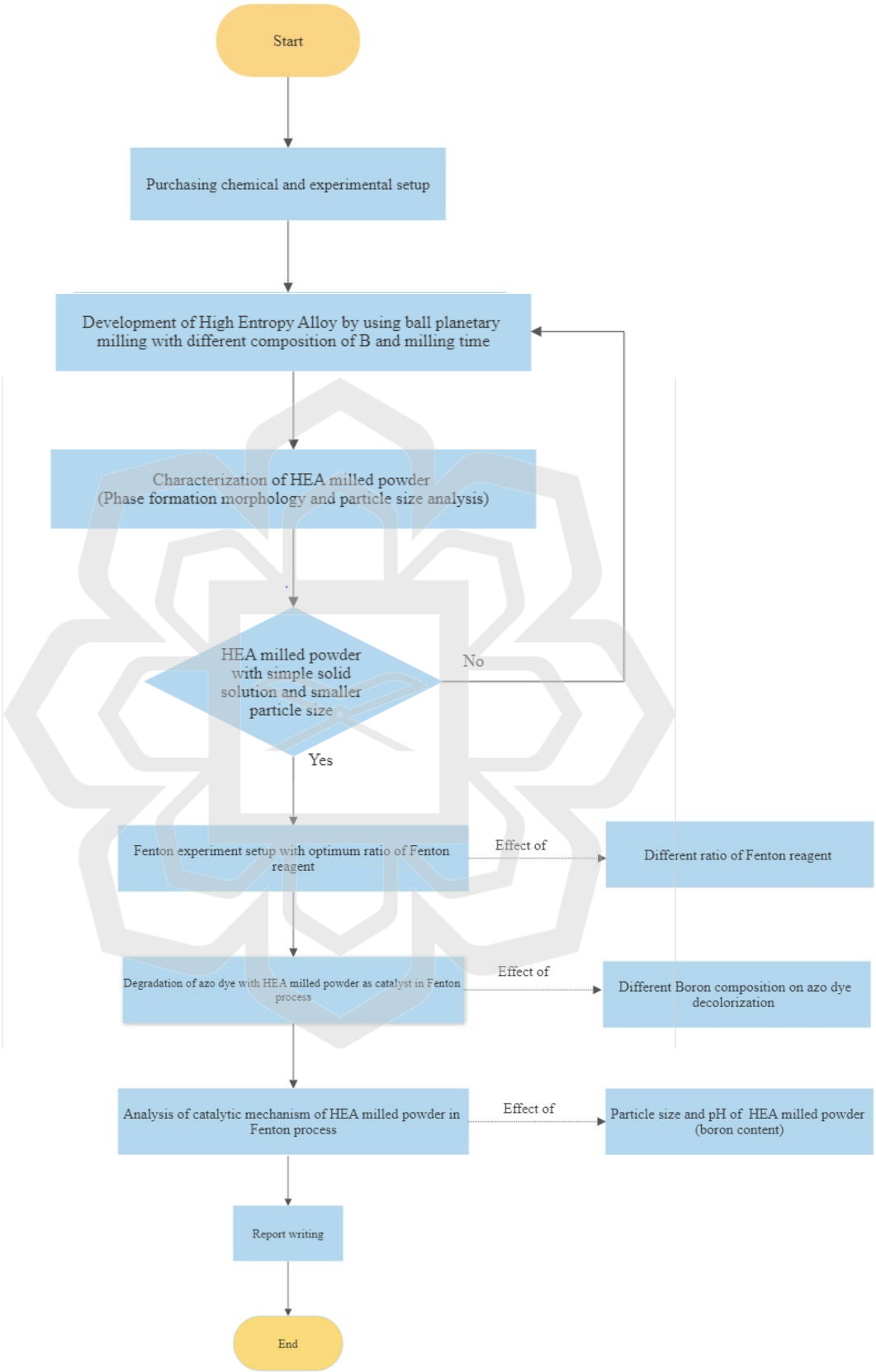

Figure 3.1 Flowchart of overall process

3.2 Materials

Material used in this study are elemental powder consist of Iron (Fe), Cobalt (Co), Nickel (Ni), Aluminum (Al), Boron (B) and Silicon (Si) that will be synthesized to form equiatomic HEAs by mechanical alloying. Other materials involved in this process are alcohol, tungsten carbide jar and ball. Moreover, the experiment set up HEA powder for performance evaluation as a catalyst to degrade the azo dye (methyl orange) required Methyl Orange azo dye (methyl orange) solution and distilled water.

3.3 Powder Preparation

Six different elemental powders were prepared with >99.9 wt% purity. The powder is weighed one by one by using weighted balance with equal mass by referring to the ball to powder ratio 5:1.

3.3.1 $FeCoNiAl_{(1-x)}B_x$ Si High Entropy Alloys

$FeCoNiAl_{(1-x)}B_x$ high entropy alloys powder is prepared from high - purity powders of Fe, Co, Ni, Al, B and Si with particles size of 100 nm. Among them, the mass fraction % of B and Al will be varied in the composition of $FeCoNiAl_{(1-x)}B_x$ HEAs powder where x = 0.00,0.02, 0.04, 0.06, 0.08 and 0.1. The composition (mass fraction wt%) $FeCoNiAl_{(1-x)}B_x$ high entropy alloys in this paper is allocated as shown in the Table 3.1.

Table 3.1 The composition (mass fraction wt%) $FeCoNiAl_{(1-x)}B_x$ high entropy alloys

Composition (mass fraction wt%) $FeCoNiAl_{(1-x)}B_x$							
High Entropy Alloy (HEA)	Code	Fe	Co	Ni	Al	B	Si
$Fe_{0.27}Co_{0.27}Ni_{0.27}B_{0.00}Al_{0.1}Si_{0.1}$	HEA-1	0.27	0.27	0.27	0.00	0.10	0.1
$Fe_{0.27}Co_{0.27}Ni_{0.27}B_{0.02}Al_{0.08}Si_{0.1}$	HEA-2	0.27	0.27	0.27	0.02	0.08	0.1
$Fe_{0.27}Co_{0.27}Ni_{0.27}B_{0.04}Al_{0.06}Si_{0.1}$	HEA-3	0.27	0.27	0.27	0.04	0.06	0.1
$Fe_{0.27}Co_{0.27}Ni_{0.27}B_{0.06}Al_{0.04}Si_{0.1}$	HEA-4	0.27	0.27	0.27	0.06	0.04	0.1
$Fe_{0.27}Co_{0.27}Ni_{0.27}B_{0.08}Al_{0.02}Si_{0.1}$	HEA-5	0.27	0.27	0.27	0.08	0.02	0.1
$Fe_{0.27}Co_{0.27}Ni_{0.27}B_{0.1}Al_{0.00}Si_{0.1}$	HEA-6	0.27	0.27	0.27	0.10	0.0	0.1

3.3.2 Calculation of Ball's Mass

The mass of the ball is being determined from the fixed mass of powder that will be carried out in this experiment which is ± 4.0 grams. Hence, the calculation of powder's mass is being calculated as below.

$$\frac{10}{1} = \frac{Mass\ of\ Ball}{4.00\ gram}$$

Mass of ball = 40 grams (approximately 5 balls)

The meaning of 10 ratios is one gram of powder is equivalent to five balls. Hence, 4.00 grams of powder is equivalent to approximately 5 balls.

3.3.3 Calculation of HEA Mass With Different Composition Of B

The mass of metal powder is being calculated based on the composition of the powder that is being set as near atomic ratio. The molecular formula for the HEAs powder is FeCoNiAl $_{(1-x)}$ B $_{x}$ Si as the composition of aluminum and boron is being varied. So, there are two type of HEAs powders with two different parameters with and without Boron which are Fe $_{0.27}$ Co $_{0.27}$Ni $_{0.27}$B$_{0.00}$Al$_{0.1}$Si $_{0.1}$ (B0.0) and Fe $_{0.27}$ Co $_{0.27}$Ni $_{0.27}$B$_{0.02}$Al$_{0.08}$Si $_{0.1}$ (B0.02). The calculation for each metal powder is being calculated by using the molar mass equation

Molar Mass = Composition × (Molar Mass) / Composition X × Molar Mass X (Eqn. 3.1)

a. Fe $_{0.27}$ Co $_{0.27}$Ni $_{0.27}$B$_{0.00}$Al$_{0.1}$Si $_{0.1}$

Example for mass for Iron powder without Boron (Fe $_{0.27}$):

$$\frac{(0.27 \times 55.85)\text{Fe}}{(0.27 \times 55.85)\text{Fe}+(0.27 \times 58.9)\text{Co}+(0.27 \times 58.69)\text{Ni}+(0.00 \times 10.811)\text{B}+(0.1 \times 26.98)\text{Al}+(0.1 \times 28.09)\text{Si}}$$

Fe 0.27 = $\frac{15.097}{52.3358}$ = 0.097 g

Table 3.2 Mass of metal powder without Boron

Type of Metal Powder	Composition	Mass (g)
Fe	0.27	0.097
Co	0.27	1.303
Ni	0.27	1.304
Al	0.00	0.224
B	0.1	0
Si	0.1	0.23

b. Fe $_{0.27}$ Co $_{0.27}$Ni $_{0.27}$B$_{0.02}$Al$_{0.08}$Si $_{0.1}$

Example for mass for Iron powder with Boron (Fe $_{0.27}$):

$$\frac{(0.27 \times 55.85)\text{Fe}}{(0.27 \times 55.85)\text{Fe} + (0.27 \times 58.9)\text{Co} + (0.27 \times 58.69)\text{Ni} + (0.02 \times 10.811)\text{B} + (0.08 \times 26.98)\text{Al} + (0.1 \times 28.09)\text{Si}}$$

Fe 0.27 = $\frac{15.097}{52.01242}$ = 1.015 g

Table 3.3 Mass of metal powder with composition of 0.02 wt% of Boron

Type of Metal Powder	Composition	Mass (g)
Fe	0.27	1.015
Co	0.27	1.070
Ni	0.27	1.068
Al	0.08	0.145
B	0.02	0.015
Si	0.1	0.189

c. $Fe_{0.27}Co_{0.27}Ni_{0.27}B_{0.04}Al_{0.06}Si_{0.1}$

Example for mass for Iron powder with Boron ($Fe_{0.27}$):

$$\frac{(0.27 \times 55.85)Fe}{(0.27 \times 55.85)Fe + (0.27 \times 58.9)Co + (0.27 \times 58.69)Ni + (0.04 \times 10.811)B + (0.06 \times 26.98)Al + (0.1 \times 28.09)Si}$$

Fe 0.27 = $\frac{15.097}{51.689}$ = 1.015 g

Table 3.4 Mass of metal powder with composition 0.04 wt% of Boron

Type of Metal Powder	Composition	Mass (g)
Fe	0.27	1.015
Co	0.27	1.078
Ni	0.27	1.075
Al	0.06	0.109
B	0.04	0.029
Si	0.1	0.190

d. $Fe_{0.27}Co_{0.27}Ni_{0.27}B_{0.06}Al_{0.04}Si_{0.1}$

Example for mass for Iron powder with Boron ($Fe_{0.27}$):

$$\frac{(0.27 \times 55.85)Fe}{(0.27 \times 55.85)Fe + (0.27 \times 58.9)Co + (0.27 \times 58.69)Ni + (0.06 \times 10.811)B + (0.04 \times 26.98)Al + (0.1 \times 28.09)Si}$$

Fe 0.27 = $\frac{15.097}{51.365}$ = 1.015 g

Table 3.5 Mass of metal powder with composition 0.06 wt% of Boron

Type of Metal Powder	Composition	Mass (g)
Fe	0.27	1.015
Co	0.27	1.078
Ni	0.27	1.075
Al	0.04	0.109
B	0.06	0.029
Si	0.1	0.190

e. $Fe_{0.27}Co_{0.27}Ni_{0.27}B_{0.02}Al_{0.08}Si_{0.1}$

Example for mass for Iron powder with Boron ($Fe_{0.27}$):

$$\frac{(0.27 \times 55.85)Fe}{(0.27 \times 55.85)Fe + (0.27 \times 58.9)Co + (0.27 \times 58.69)Ni + (0.04 \times 10.811)B + (0.06 \times 26.98)Al + (0.1 \times 28.09)Si}$$

$$Fe\ 0.27 = \frac{15.097}{51.689} = 1.015\ g$$

Table 3.6 Mass of metal powder with composition 0.08 wt% of Boron

Type of Metal Powder	Composition	Mass (g)
Fe	0.27	1.015
Co	0.27	1.078
Ni	0.27	1.075
Al	0.02	0.109
B	0.08	0.029
Si	0.1	0.190

f. $Fe_{0.27}Co_{0.27}Ni_{0.27}B_{0.00}Al_{1.00}Si_{0.1}$

Example for mass for Iron powder with Boron ($Fe_{0.27}$):

$$\frac{(0.27 \times 55.85)Fe}{(0.27 \times 55.85)Fe + (0.27 \times 58.9)Co + (0.27 \times 58.69)Ni + (0.04 \times 10.811)B + (0.06 \times 26.98)Al + (0.1 \times 28.09)Si}$$

$$Fe\ 0.27 = \frac{15.097}{51.689} = 1.015\ g$$

Table 3.7 Mass of metal powder with composition 0.10 wt% of Boron

Type of Metal Powder	Composition	Mass (g)
Fe	0.27	1.015
Co	0.27	1.078
Ni	0.27	1.075
Al	0.00	0.109
B	0.10	0.029
Si	0.10	0.190

3.4 Planetary Ball Milling

The project starts with the mechanical alloying process by using a Fritsch Pulverisette P-5 planetary ball milling with high purity argon atmosphere. There are three parameters that are considered which are duration of milling, PCA and speed of milling.

The power supply at the machine is switched on and the mixture of iron (Fe), cobalt (Co), nickel (Ni), aluminum (Al), boron (B) and silicon (Si) powders are put in the grinding bowl. The first run is done for the HEAs powder without the presence of boron $Fe_{0.27}$ $Co_{0.27}$ $Ni_{0.27}B_{0.00}Al_{0.08}Si_{0.1}$ (B0.00). The speed, repetition moment, rotating and pause time for the machine was set as shown in Table 1. The most important part is that the bowl must be fixed to ensure it fastens and clamps into the machine chamber before closing the chamber for safety issues. The experiment was repeated for different milling times as stated in Table 3.1. After finishing the experiment and obtaining the product, the sample is taken out from the grinding bowl. Then, the experiment was repeated for $Fe_{0.27}$ $Co_{0.27}Ni_{0.27}B_{0.02}Al_{0.08}Si_{0.1}$ (B0.02), $Fe_{0.27}$ $Co_{0.27}Ni_{0.27}B_{0.04}Al_{0.1}Si_{0.1.}$ (B0.04), $Fe_{0.27}$ $Co_{0.27}Ni_{0.27}B_{0.02}Al_{0.08}Si_{0.1}$ (B0.06), $Fe_{0.27}$ $Co_{0.27}Ni_{0.27}B_{0.02}Al_{0.08}Si_{0.1.}$(B0.08) and $Fe_{0.27}$ $Co_{0.27}Ni_{0.27}B_{0.00}Al_{1.00}Si_{0.1}$ (B1.0) Next , the HEA powders were characterized by SEM, XRD, EDS, FESEM, Zetasizer Analysis and CHNS Analyzer.

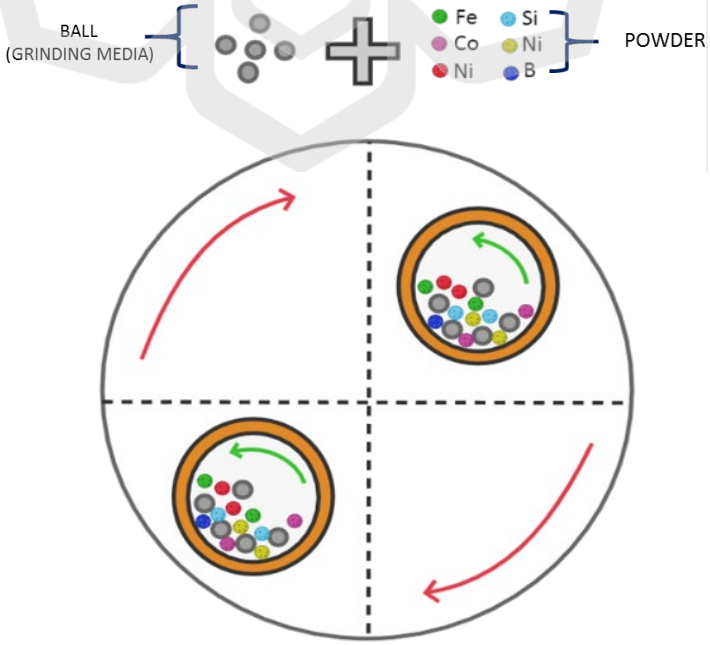

Figure 3.2 Experimental Design of Planetary Ball Milling

Table 3.8 Constant and Manipulated Variables of Milling Process

Constant Parameter		**Manipulated Variables**		
Milling Speed	350 Rpm/min	**Milling Time / Hours**	**Cycles**	**Pause Time/Mins**
Number of Balls	5	10	60	5
		20	120	5
Mass of sample powder	± 4.00 g	30	180	5
		40	240	5
		50	300	5
		60	360	5
		70	420	5
		80	480	5
		90	540	5
		100	600	5
		120	720	5
		140	840	5
		160	960	5

3.5 Fenton Process

The experiment setup for catalytic performance is shown in Figure 3.3. The Fenton reagent consists of hydrogen peroxide and the ferrous ion, Fe2+. The ferrous (II) sulphate heptahydrate salt, FeSO4 • H2SO4, was used to react with the hydrogen peroxide. The dye solution was created by mixing water with 50 mg/l of methyl orange powder. The pH of methyl orange solution was then brought down to 3 by adding diluted sulfuric acid and sodium hydroxide. Then, HEA, H2O2, and FeSO4 are added into methyl orange solution. The investigation involves modifying parameters such the concentration of hydrogen peroxide, the amount of ferrous sulphate heptahydrate, and the percentage of boron (B) in HEA. In every run carried out, the degradation efficiency for each variable is calculated and recorded. The variables are included in Table 3.8.

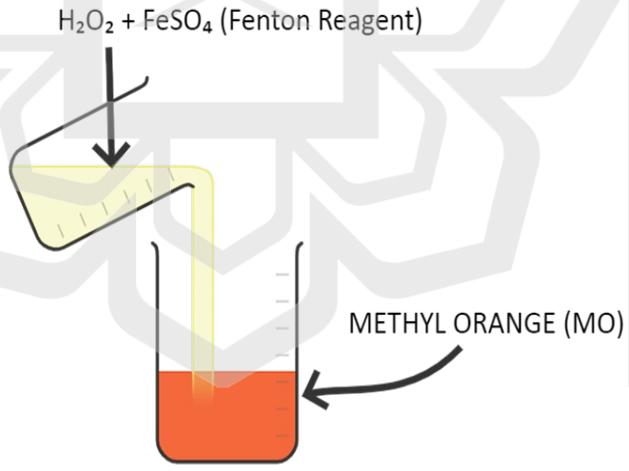

Figure 3.3 Schematic diagram of Fenton process setup

Table 3.8 Type of runs of Fenton Process with different manipulated variables

RUN	FACTOR 1: HYDROGEN PEROXIDE CONCENTRATION (M)	FACTOR 2: VOLUME OF IRON SULFATE (ml)
1	0.3	15
2	0.1	10
3	0.3	10
4	0.1	5
5	0.2	10
6	0.2	15
7	0.3	5
8	0.2	10
9	0.1	15
10	0.4	5
11	0.4	10
12	0.4	15
13	0.5	5
14	0.5	10
15	0.5	15

The performance of HEA powders as a catalyst in the Fenton process was then carried out with the optimum amount of hydrogen peroxide and ferrous sulfate. The experimental set up and HEAs powder variables were shown in Figure 3.4 and Table 3.3 respectively. The catalytic performance of HEA in Fenton's process was then characterized and tested by visual observation, UV-Vis and degradation efficiency.

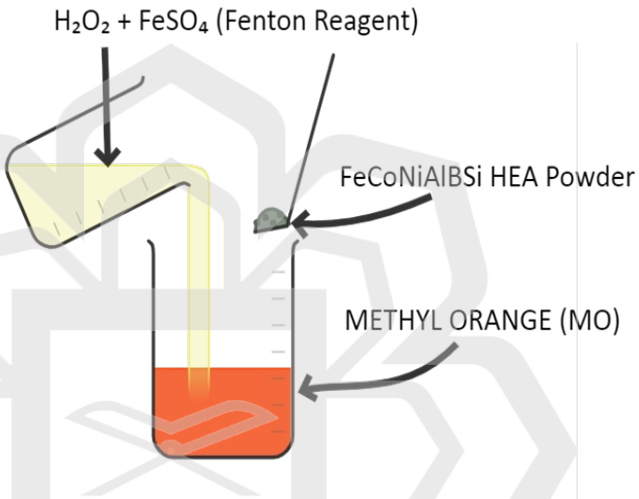

Figure 3.4 Schematic diagram of Fenton process setup with HEA as a catalyst

Table 3.10: Type of runs of Fenton Process with different manipulated variables

Constant Variable	Manipulated Variable
• **50mg/l of Methyl Orange** • **pH: 3** • **Room Temperature** • **10ml of Iron (II) Sulphate** • **0.1M Concentration of Hydrogen Peroxide** • **Mass of HEA (0.01g)**	• FeCoNiAlBSI (B=0.00) • FeCoNiAlBSI (B=0.02) • FeCoNiAlBSI (B=0.04) • FeCoNiAlBSI (B=0.06) • FeCoNiAlBSI (B=0.08) • FeCoNiAlBSI (B=0.10)

3.6 Kinetic Reaction of HEAs Powder as a Catalyst in Fenton Process

Adsorption kinetics modeling is used in this research to have a better understanding of the HEA kinetic mechanism as a catalyst in the Fenton process. Arhenius equation (A.-R.A. Giwa et al. 2020) is used to plot pseudo first order kinetic reaction and pseudo second order kinetic reaction.

Pseudo first order kinetic:

$$\ln\frac{Ao}{At} = -kdt \quad \text{(Eqn 3.1)}$$

Pseudo second order:

$$\frac{t}{A_t} = \frac{1}{k_2 A_e^2} + \frac{t}{A_e} \quad \text{(Eqn 3.2)}$$

3.7 Characterizations of HEA Powder

3.7.1 X-Ray Powder Diffraction (XRD)

X-ray powder diffraction (XRD, D2) manufactured by Bruker is a rapid analytical technique used primarily to identify the phase of a crystalline material and provide information on the unit cell size. The material analyzed was finely ground and homogenized before it was put in the sample holder. The XRD analysis was performed in the range of 20 to 100Θ with 0.025 step size.

3.7.2 Field Emission Scanning Electron Microscope (FESEM)

A field emission scanning electron microscope (FESEM, ZEISS MERLIN, STEM Mode) provides topographical and elemental information especially for nanomaterials powder at high magnification of 10x to 300000x with virtual unlimited depth of field. Compared with conventional scanning electron microscopy (SEM), field emission SEM (FESEM)

produces clearer, less electrostatically distorted images with spatial resolution down to 1 1/2 nanometers which is three to six times better. In this work, FESEM was carried out in order to clearer morphology of nanomicrostructure.

3.7.3 Scanning Electron Microscope (SEM)

A scanning electron microscope (SEM, JSM-IT100) manufactured by JEOL is a type of electron microscope which produces sample images by scanning the surface with a focused electron beam. The electrons communicate in the sample with atoms, creating different signals containing information about the topography of the surface of HEAs powder.

3.7.4 Energy Dispersive X-Ray Spectroscopy (EDS)

EDS analysis is also known as energy dispersive X-ray analysis or energy dispersive X-ray microanalysis. This characterization method is being used for the elemental analysis or chemical of a sample powder. This method enables the analysis of near-surface elements and the amount at different positions providing a map of the sample.

3.7.5 Particle Analysis Zetasizer

Zetasizer (Malvern ZEN 360 Nano ZS) was applied for measurement of nanoparticles. It can analyze the particle size and size distribution of HEA powder by dynamic light scattering (DLS) method, which measures the frequency shift of laser light reflected by particles in suspension moving by Brownian motion. The distribution of particle speed was converted to a size distribution. The measurement range for size distribution was from 6 nm to 6 microns.

3.7.6 CHNS Analyzer

CHNS analyzer will be used to determine the exact concentration of carbon and hydrogen in the HEA milled powder that might be present due to oxidation that is generated during the milling process. CHNS elemental analysis is based on the combustion of the sample. These combustion products are measured using gas chromatography and thus the ratio of the elements in the original sample is determined.

3.8 Performance of HEAs As a Catalyst in Fenton Process

3.8.1 Visual Observation

Visual observation will be carried out before, during and after the degradation process on the azo dye (methyl orange) solution by observing the color changes over time and the dissolution produced.

3.8.2 Ultra-Violet Visible Spectroscopy

The absorbance spectrum will be analyzed by using UV-Vis spectrum scanning (UV Line 9400) machine where an excitation wavelength is 250nm-600nm. This spectroscopy will identify and measure the concentration of the substance that has been emitted from or absorbed by the azo dye (methyl orange) during the Fenton reaction. The absorbance of the azo dye (methyl orange) at different reaction times can be converted into degradation efficiency.

3.8.3 Degradation Efficiency

Azo degradation efficiency in the Fenton process can be estimated by using this formula, $D\ (\%) = \frac{C_0 - C_t}{C_0}$ where C_0 and C_t correspond to the initial dye concentration and the concentration of dye at the reaction time, t respectively.

3.9 Summary

In this chapter, mechanical alloying method namely ball milling was used to alloying six elements of the high entropy alloys to obtain simple solid solution (FCC and BCC) phase. Several characterizations techniques such as XRD, SEM, CHNS and particle sizes have been performed to acquire the characteristics of the alloy. Next the Fenton experiments was done with different amount of Fenton reagent to find the optimum parameter for the next process. The HEA powders was used as a catalyst to improve the efficiency of the Fenton process. The performance of the HEA powders as catalyst was investigated by visual observations and UV-vis machine. In order to determine the kinetic efficiency of the HEA powders as catalyst, the degradation efficiency was calculated using Ahernius equation.

CHAPTER FOUR

RESULTS & DISCUSSION

4.1 Design of FeCoNi $(B_xAl_{1-X})_{0.1}Si_{0.1}$ High Entropy Alloy as Catalyst

The multicomponent FeCoNiAlBSi was developed by Nordin et al. (2022) in as-cast form based on the HEA principle of HEA empirical rules described by Yeh et al. (2004), where the constituent elements are in equal or near equal concentrations and not contain any host elements. The percentage of each element involves in the study was calculated based on a well-known Miedema's model (Akira et al, 2005) and Hume Rothery rules (Cantor et al., 2004) in order to obtain the solid solubility formation in the system.

In this study, the HEA was re-produced by planetary ball milling in powdered form starting from 0H up to 160H until all elements diffused to become solid solutions and homogenous. Boron was varied to reduce the stability of the disordered BCC solid solution, promoting the formation of secondary phases; Fe2B and BCC/B2 (Nordin et al. 2022). In term of catalytic points of views, J. Ramirez et al (1995) suggested that the presence of B in alloy increases hydrogen concentration that affect the acidic environment in the Fenton process. Thus, the study on the HEA with the variation of boron in degrading azo dye was performed in this work.

Selection of the six elements in this study was mainly related for the degradation of azo dye in the Fenton process. For example, Fe is the most commonly used as Fenton active element, with the highest Fenton-like activity in acidic environments; Co is the neutral Fenton active element, with Lewis acidic, which is not only beneficial to promote Fenton-like effects in neutral/near-neutral environments, but also beneficial to increase Fenton-like

activity by lowering pH without adding acid; Ni is a stable metal element that can improve the catalytic stability of the alloy catalyst; Aluminium, according to Mujika et al. (2014), can promote Fenton reaction by induce the formation of OH radicals via the Fenton reaction and the presence of Boron in the Fenton process facilitates the electron transfer process and causes the reduction of some Fe(III) to Fe(II) species, improving the system's kinetics and forming a greater number of oxidizing species, leading to the formation of reactive catalysts for Fenton chemistry.

However, aluminum has low adsorption properties as catalyst and aluminum need combine with other metals in other to improve its catalytic activity (Duan et al., 2012). Further to that, the addition of P, C, B, O, and Si may improve the electro-catalytic properties of Aluminum by modifying the crystal structure and generating new active sites. The B atoms in this work transferred some electrons to the adjacent metal atoms, enriching the population of metal sites and improving catalytic activity (Ran Wei et.al, 2021). Besides, according to J. Ramirez et al. (1995), the presence of B in alloy raises hydrogen concentrations, which affects the acidic environment in the Fenton process. This scenario involves condensation reactions between B-O-H groups that are close to one another and A1-OH groups that have a higher boron content. the population of metal sites and improving catalytic activity (Ran Wei et.al, 2021). Thus, the vary composition of Boron and Aluminum in $FeCoNi(B_xAl_{1-x})_{0.1}Si_{0.1}$ high entropy alloy may affect the catalytic activity of HEA powder and the acidic environment in the Fenton process during methyl orange (MO) degradation process.

4.2 Crystal Structure Effect to the Milling Time

XRD patterns of HEA powders at various milling periods are shown in Figure 4.1. Multiple peaks for each element can be found in the unmilled sample at 0H, indicating polycrystalline mixtures of the element powders where diffusion has not yet taken place. After 5 hours of milling, the peaks for B, Si, Co, Ni, and Al begin to fade as a result of element diffusion into the iron matrix. The decline in peak height is also caused by the reduction in lattice strain and crystallite size. The BCC phase was gradually being eliminated, and at 15H the FCC phase started to form. The Fe peaks at 0H shift toward smaller angles as a result of the lattice expansion brought on by the elemental diffusion of B, Si, Co, Ni, and Al, which resulted in the synthesis of FCC and BCC/B2 after 30H. When the milling time is greater than 70H, there are just two simple phases which are FCC and BCC.

Figure 4.2 illustrates how the interaction between Fe and B in HEA-3 caused the intermetallic iron boride (Fe2B) to form after B was added to the compound. Due to the low weight % of B in the HEA-2 powder, the Fe2B phases did not manifest in the HEA-2 crystal structure. Thus, after 160 hours of milling, three phases are discovered in HEA-1 and HEA-2: FCC, BCC, and BCC/B2, whereas three phases are identified in HEA-3, HEA-4, HEA-5 and HEA-6: FCC, BCC/B2 and Fe2B.

According to Moravcik et al. (2020), the presence of the oxygen in the milled powder may come from the ethanol used as PCA in the milling process. The study also claimed that, oxygen, in the form of various oxides, is already present on the surfaces of raw powders. The oxides are formed as a result of the reaction of metallic surfaces with ambient

air. The oxide layer forms on the surfaces of metals during powder manufacturing and can grow during storage. Besides, elements with a high affinity for oxygen, such as iron in our case, are prone to oxidation. However, there are not significant peak of oxygen in the XRD pattern of HEA milled powder as shown in Figure 4.1 and Figure 4.2 compared to solid solution peaks such as FCC, BCC, BCC/B2 and Fe2B. Thus, the XRD (Figure 4.1 and Figure 4.2) analyzed that there was no significant contamination in the HEA powder from the milling process.

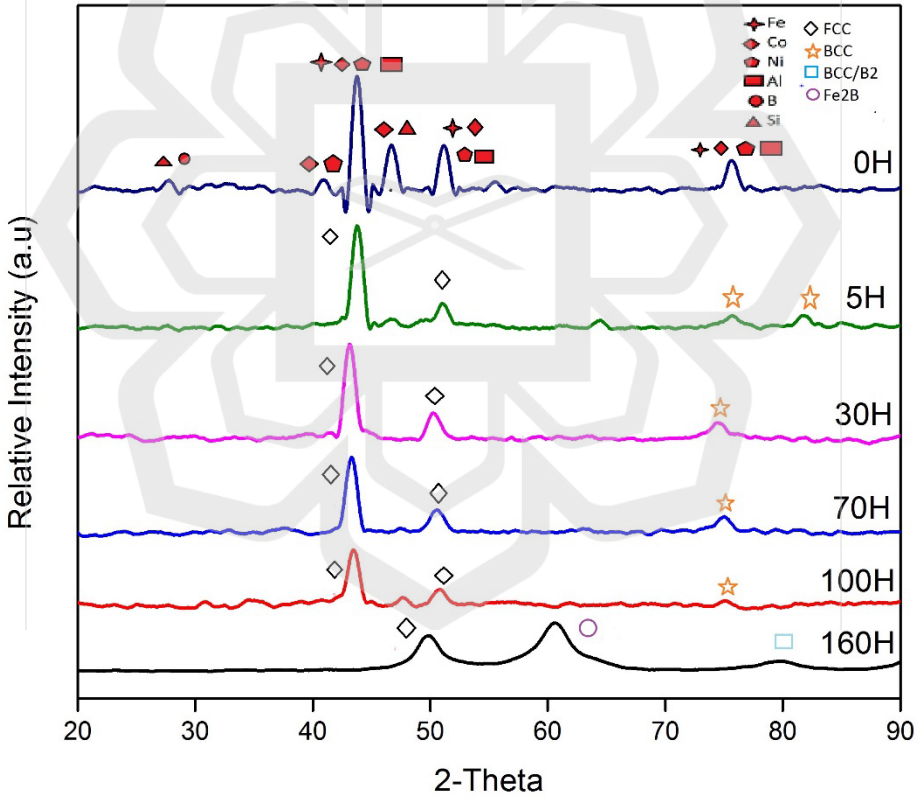

Figure 4.1 XRD patterns of HEA-6 powder at different milling time

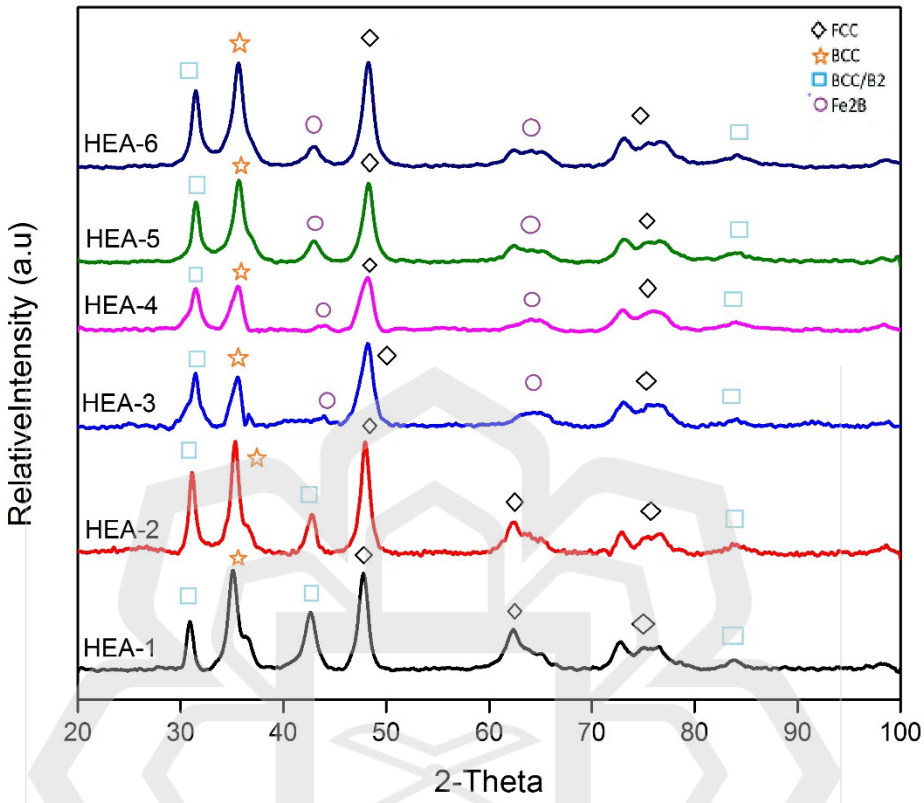

Figure 4.2 XRD patterns of HEA powder with different composition of B at160H

4.3 Morphological Effect to The Milling Time

4.3.1 Scanning Electron Microscopic (SEM)

Morphological studies on HEA powder were conducted from 0 to 160 hours of milling time. The particle size of HEA powder was observed to increase from 0.960 µm at 5H to 1.167 µm at 30H milling times. The fact that milled powders agglomerate during high intensity milling is proof of this, and research on particle disruption homogeneously is currently underway. Figure 4.3 shows the morphological changes of milled HEA powder particles over time. Because the particles in Figure 4.3 (a) are spherical and non-separated, there was no discernible deformation. The particles began to fracture during the early hours of milling, and cold welded became prominent, leading to agglomeration. Figure 4.3 (d) and Figure 4.3 (e) show an increase in the average particle size of HEA powder at 70H and 100H, which are 1.344 µm and 2.000 µm, respectively, where the particles formed irregular forms with no geometric regularity. These significant changes are caused by strong plastic deformation and the force of a ball-powder-ball impact into the particles. The cold welding effect aids in atom diffusion during the alloying process. The particle size of the HEA powder reduces to 0.943 µm at 160H. As a result, when the milling process is prolonged, these agglomerations are crushed down into smaller, more uniformly sized, and flattened particles, as seen in Figure 4.3 (g). This is due to the fact that the equilibrium between fracture and cold welding is reached after a specific amount of milling time. HEA powder is effected to be one of the micro-nanostructured materials with amazing chemical and catalytic properties. Figure 4.3 (g) shows HEA powders with a rough surface and many corrugations and micro pores, indicating a large specific surface area and a large number of active sites. As a result, the smaller particle size of HEA powder has a bigger surface

area and higher residual strain, enhancing the catalytic activity efficiency of HEA (Wu et. al, 2019).

MORPHOLOGY OF HEA POWDER OVER MILLING TIME

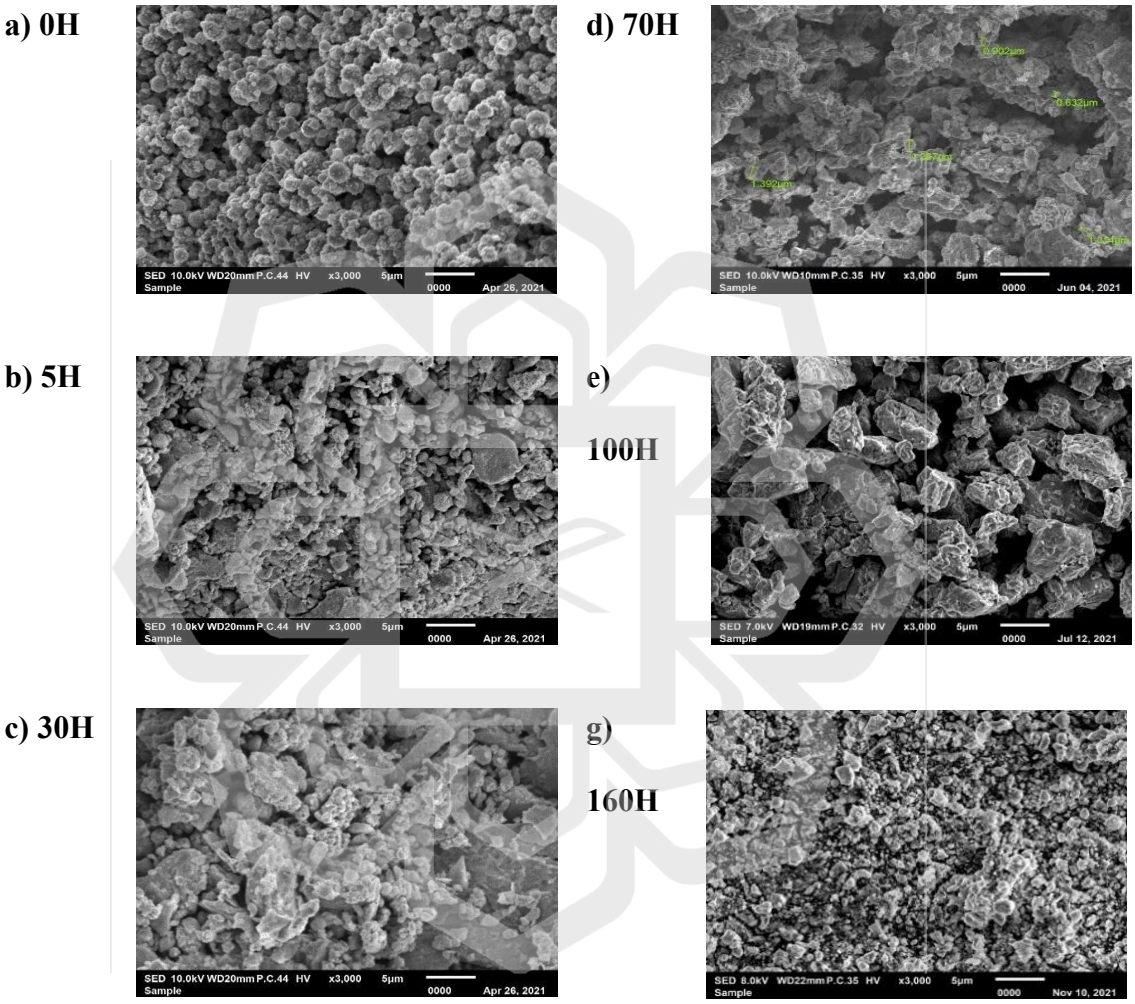

Figure 4.3. Scanning electron microscope (SEM) image of HEA powder at 3000x magnification where a) 0H, b) 5H, c) 30H, d) 70H, e)100H, f)100H, and g)160H

Figure 4.4a shows that the SEM micrograph of the milled HEA powder at 3000x magnifications. While figure 4.4b shows the SEM image composition mapping with Fe, Co, Ni, Al, B and Si constituents elements were distributed uniformly. This images showed excellent homogeneity on the microscale level of the alloys. Table 4.1 shows the EDS results based on wt% and at%. It showed that, the value is approximately similar to the proposed composition. However, it was noted that the EDS machine was not able to detect boron due the low atomic number of B. The element with atomic number less than Sodium (Na) cannot be detect using EDS. It was also noted that the oxygen also can be detected in the alloy which shows the presence of impurities during the increasing of milling times.

Table 4.1: Wt% of HEA milled powder from EDS

ELEMENT	WT%	AT%
CO	44.12	37.60
FE	21.14	19.01
NI	20.15	17.23
B	0.00	0.00
AL	0.83	1.55
SI	13.76	24.61
O	15.37	40.60

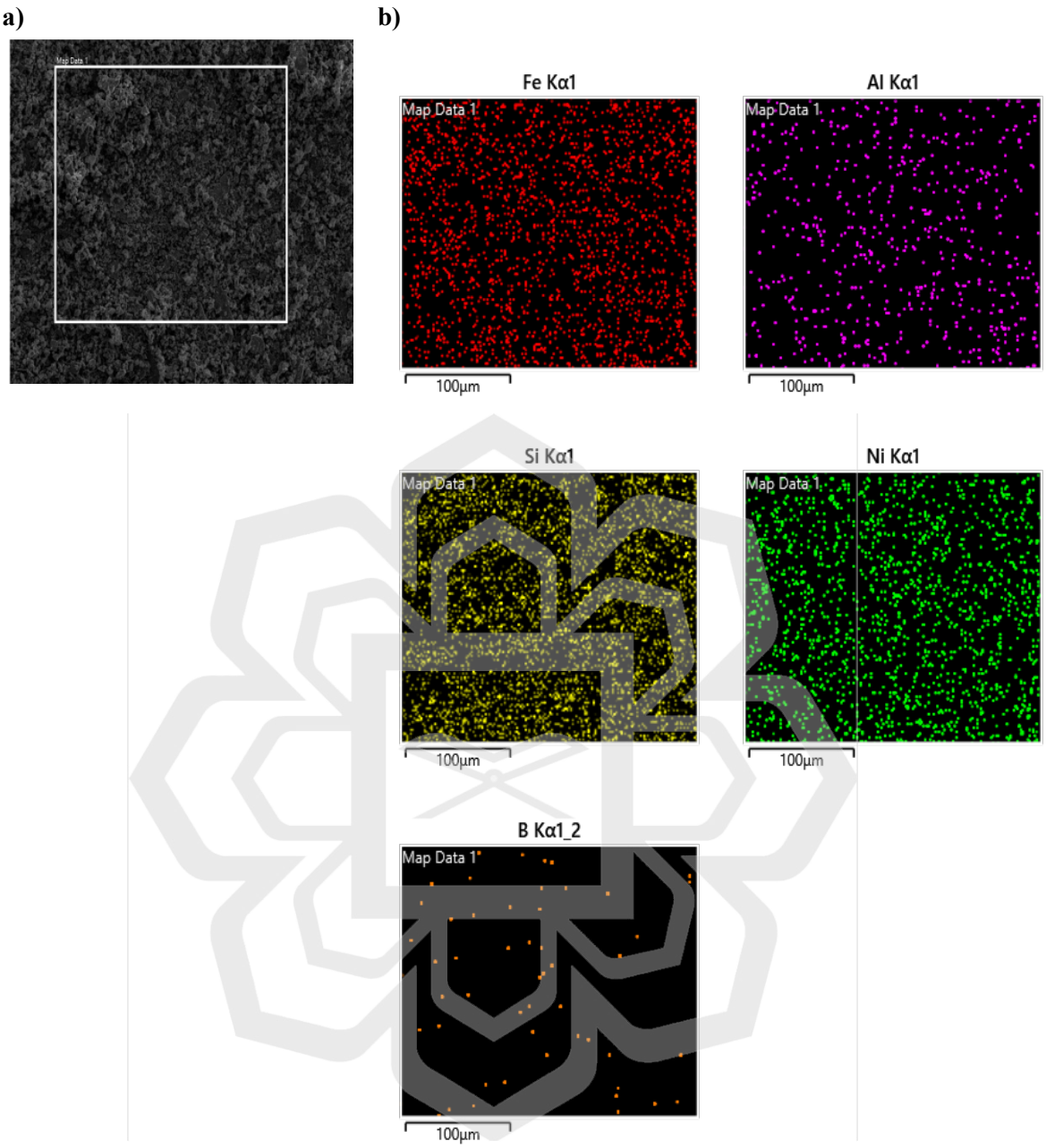

Figure 4.4: a) SEM micrographs of the milled powder of HEA FeCoNiAlBSi b) mapping constituents element Fe,Co,Ni,Al,B,Si

4.3.2 Field Emission Scanning Electron Microscope (FESEM)

The excellent catalytic characteristics of many nanostructured materials are plainly reliant on their morphologies, crystallite size, and distribution. The HEA milled powder exhibit a rather uniform distribution at 160H of milling, as shown in Figure 4.5a while Figure 4.5b shows that the surface of the HEA milled powder is rough, with numerous corrugations and micropores. The results show that the HEA milled powders have a high specific surface area with a lot of active sites (Shi Kai Wu et al.,2019). Thus, it will help in improving catalytic activity in degrading azo dye (methyl orange).

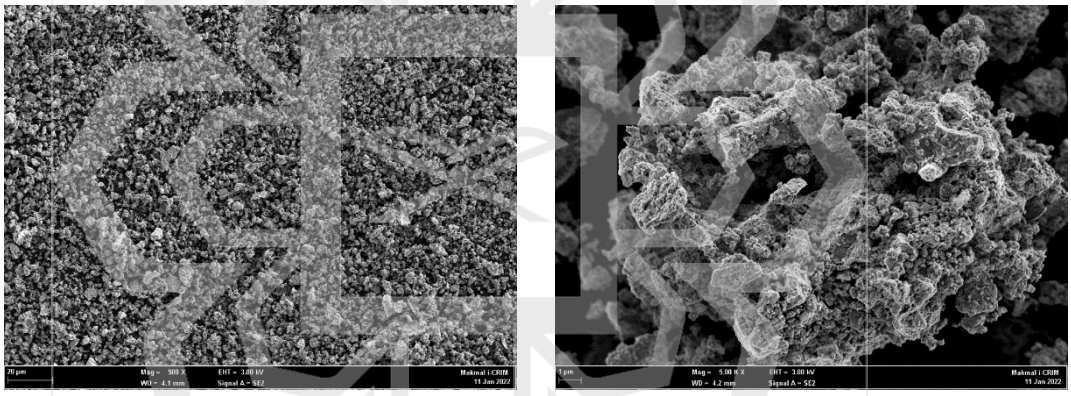

a) **b)**

Figure 4.5 Morphology of HEA milled powder at 160H of milling time

4.3.3 Particle Size Analysis

The change in particle size over the course of milling is shown in Figure 4.6. As shown in Table 4.2, the strain hardening and powder fracture that occur during the milling process cause the particle size to decrease at 5H of milling which is 0.960 μm. However, due to the influence of strong centrifugal forces caused by the opposing directional rotation of the bowl and turn disc, which result in the accumulation of the powder, can be linked to

an increase particle size as the milling increases especially at 30H, 70H and 100H of milling times 1.167 µm, 1.344 µm and 2.000 µm respectively. As the milling time increase until 160H of milling, the particle size decreases until 0.943 µm. The figure 4.2 demonstrated that the decrease in particle size at 160H of milling is caused by the elements diffusion into solid solutions, which strengthens them.

Investigated were the effects of milling duration on the evolution of structure and morphology. When the combined powder is ball milled for 160 H, BCC/B2 and Fe2B solid solution structure phases are obtained; these phases did not appear at 5H of milling time (refer section 4.1). Compared to 5H milled powder of HEA, the HEA milled powder made from the 160 H ball mill exhibits a fine morphology and excellent homogeneity (refer section 4.2). Thus, FeCoNiAlBSi HEA solid solution phases at 160H of milling promote excellent catalyst properties of in Fenton process with a particle size of less than 1 µm; the 160 H ball milled powder is composed of hard agglomerations of nanosized crystalline and homogenous particle dispersion. It is reported by Zv et al., (2016) and Wu et al., (2019), average particle size of high entropy alloy (HEA) powder can degrade azo dye in solution is in between 1-20 µm.

Table 4.2: HEA milled powder particle size over milling

HEA-powders over milling time (H)	**Average powder particle size (µm)**
5	0.960
30	1.167
70	1.344
100	2.000
160	0.943

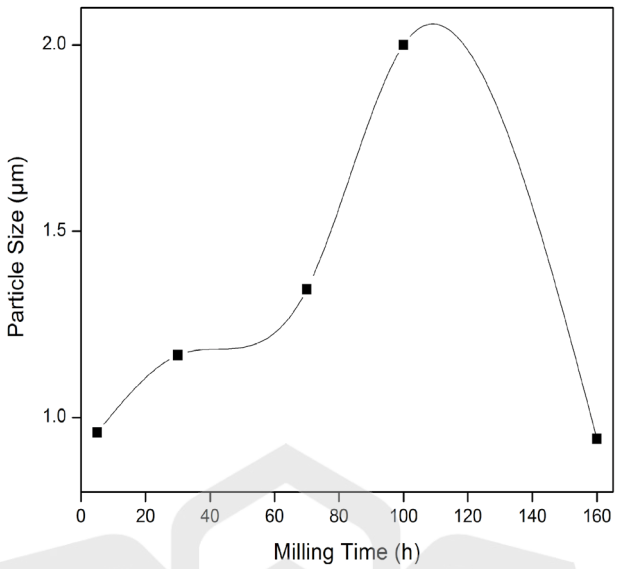

Figure 4.6: Graph of particle size of HEA milled powder over milling time

3.1.1.1 ELEMENTAL ANALYSIS

CHNS was carried out in order to investigate further the presence of impurities on HEA milled-powder due to increasing of milling time as shown in Table 4.3, milling time increase, carbon and hydrogen composition increases respectively. The presence of constituent element on the HEA milled-powder is due to friction between element and tungsten ball (Moravcik et al., 2020). The oxygen value was estimated by EDS analysis and it was found that the value is 15.37 wt% at 160H milling times as shown in Table 4.1. However, the value of C and H is considered very low (less than 2% C) and the C, O and H constituent elements can be neglected since it will be not affected the performance of the HEAs as catalyst.

Table 4.3 Elemental analysis of the HEA milled powder at 100H, 140H and 160H of milling time

ALLOY CODE	MILLING TIME (H)	CHNS ANALYZER			
		C	H	N	S
HEA-2	**100**	**0.82**	**0.18**	**0**	**0**
HEA-2	**140**	**1.57**	**0.31**	**0**	**0**
HEA-2	**160**	**1.91**	**0.26**	**0**	**0**

4.4 Degradation Efficiency of Azo Dye (Methyl Orange) In Fenton Process

Two reagents, hydrogen peroxide (H_2O_2) and ferrous (II) sulphate ($FeSO_4$), have a significant impact on the Fenton process. Ferric ions (Fe^{2+}) and hydroxyl radicals (OH^-) are the products of the reaction between these two reagents. The hydroxyl radical is crucial in the Fenton reagent's attack on the methyl orange dye molecule because it weakens the amine link, which aids the decolorization dye in the solution.

Iron (II) ion (Fe^{2+}) and H_2O_2 both behave as OH^- scavengers in addition to interacting to produce OH^- The rate of OH^- production and scavenging should be influenced by the ratio of [Fe^{2+}] to [H_2O_2]. As a result, it is essential to select the best [Fe^{2+}] / [H_2O_2] ratio feasible (A.R.A, Giwa et al.,2020). The constant concentration 50mM of methyl orange, MO, was investigated at varied hydrogen peroxide (H_2O_2) and ferrous (II) sulphate ($FeSO_4$), concentrations to establish molar ratios of 10:1.02 - 3:1.02 in order to ascertain the ideal starting concentration ratio of [Fe^{2+}] / [H_2O_2] on the removal of MO. This ratio The ideal molar ratio in this experiment was found to be 10:1.02, as shown in Figure 4.7.

The outcomes were remarkably similar to those found in the literature on Fenton process in degrading azo dye (methyl orange), which found that the best conditions involved a ratio of 1:10 iron to hydrogen peroxide (Burbano et al., 2003).

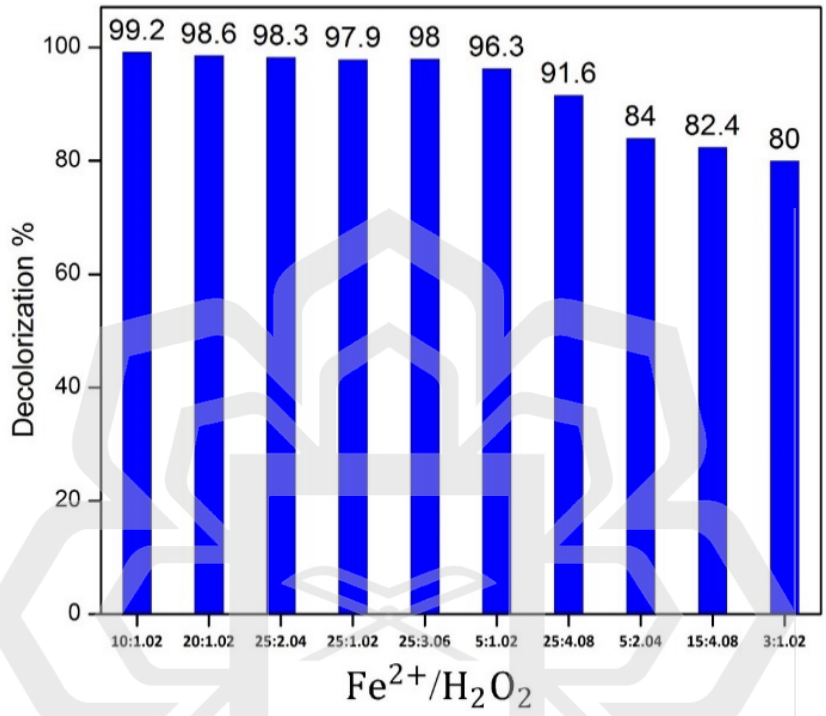

Figure 4.7: Decolorization percentage with different ratio of Fenton reagent

Figure 4.8 Visual observations of a) before the Fenton reaction and b) after Fenton reaction

Figure 4.8 shows the visual observation before and after Fenton process which showed within 60 minutes of reaction the methyl orange turned into colourless solution.

The Fenton process is significantly influenced by the reagents ferrous (II) sulphate ($FeSO_4$) and hydrogen peroxide (H_2O_2). The interaction of these two substances results in the formation of hydroxyl radicals and ferric ions. Hydroxyl radical plays an important role in Fenton reagent to attack the molecule of methyl orange dye and degrades the amine bond which helps the decolorization dye in the solution which can be seen in the figure 4.8b (Nur Hudawiyah Abu Hassan et al., 2021). Sludge formation in Fenton process usually occur after neutralization process due to ferric sludge. Contrary in this study, the production of ferric sludge was done by visual inspection and from Figure 4.8 (b) not ferric sludge is produced after the degradation process.

4.4.1 Effect of Particle Size

Particle size and homogenous dispersion of HEA powder are the biggest influence in the degradation efficiency of azo dye (methyl orange) in the Fenton process. Table 4.4 shows that the degradation efficiency of azo dye (methyl orange) in the Fenton process is 99% when the particle size of HEA powder catalyst is 0.943um. This scenario shows that, as the milling time increases, the particle size decreases and increases the surface area of HEA where it exhibits a more active site for HEA powder. Besides, the particle sizes of the HEA powders at 160H have a homogenous distribution with many corrugations and micro-pores, as shown in Fig. 4.7(g). These findings suggest that the three HEA powders have large specific surface areas and promotes more active sites (Miracle, DB, 2019) thus enhance the Fenton process with presence of HEA powder as catalyst.

Table 4.4 Azo dye (methyl orange) degradation in Fenton process with different particle size of HEA powder over milling time

MANIPULATED		**RESPONDING**
MILLING TIME (H)	**PARTICLE SIZE (µM)**	**DEGRADATION EFFICIENCY (%)**
5	0.960	93.84
70	1.344	92.87
160	0.943	99.00

4.4.2 Effect of PH

Figure 4.10 depicts that HEA-2 with the presence of B have higher degradation efficiency which is 99%, compared to HEA-1, HEA-3, HEA-4, HEA-5 and HEA-6 which are 96.68%, 96.4%, 95.8%, 91.5% and 89.3% respectively, within one hour of Fenton reaction. Figure 4.11 shows correlation between decolorization and pH value with increasing boron composition in HEA milled-powder. Overall, it can be that as the boron composition increases, the pH value of increases and decolorization efficiency decreases. However, it was found that for HEA-2 has highest degradation efficiency which is 99% with 6.1 pH value. It can be concluded that, Fenton process with HEA-2 composition has highest efficiency in terms of pH factor. Meanwhile, HEA-6 has the lowest degradation efficiency with 5.2 pH value.

J. Ramirez et al (1995) suggest that the presence of B in alloy increases hydrogen concentration that affect the acidic environment in the Fenton process. This scenario associated with condensation reactions between close B-O-H groups and A1-OH groups

with increasing boron composition. However, excessive acidic environment may depict the reaction of the Fenton process (A.R.A, Giwa et al., 2020). Due to this reason, HEA-6 has lower degradation efficiency compared to HEA-2.

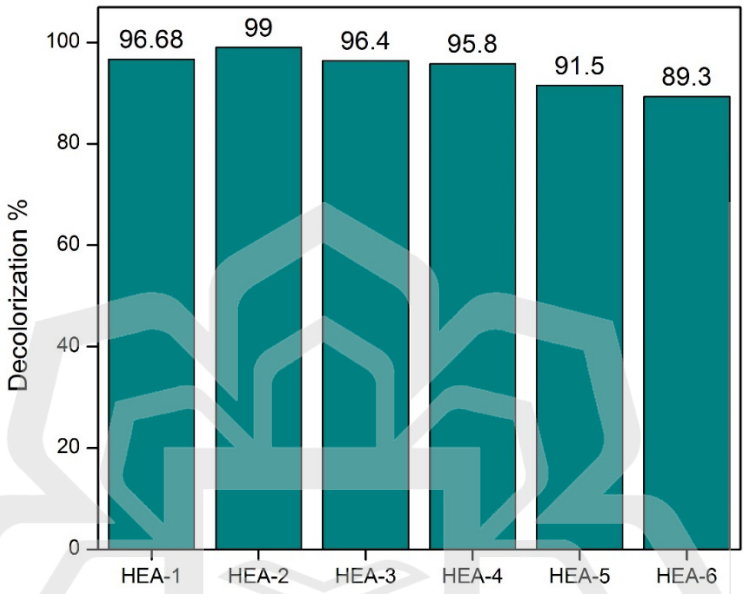

Figure 4.10 Degradation of Azo dye (methyl orange) with different composition of B in HEA milled powder as catalyst in the Fenton process

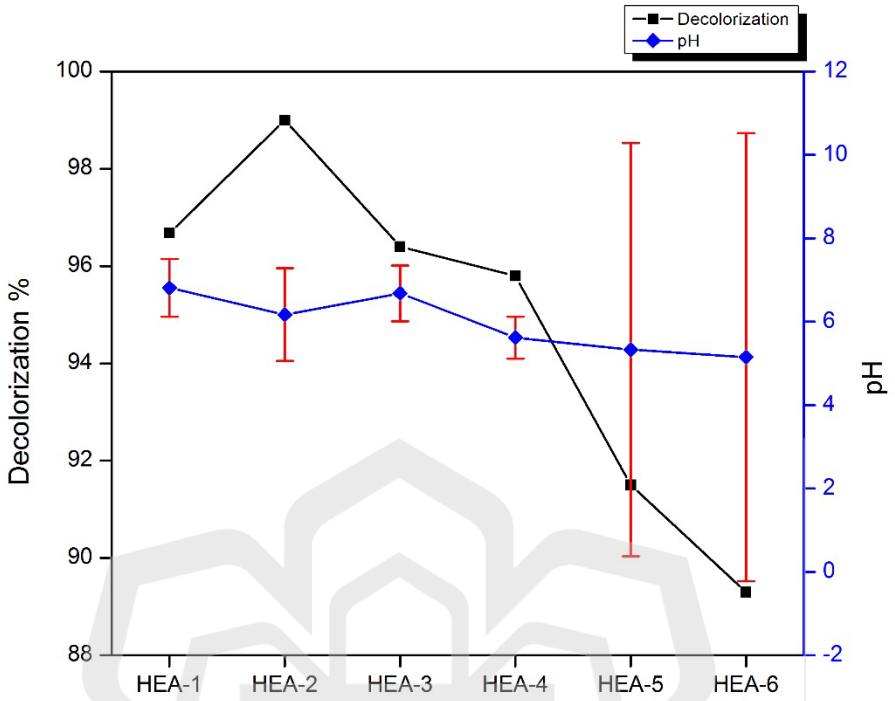

Figure 4.11 The relation between HEA milled powder pH and decolorisation percentage.

4.5 Decolorization Kinetics Of Azo Dye (Methyl Orange) With HEA as Catalyst

The degradation of the azo dye (methyl orange) in this study, as in earlier research, was specified by a pseudo first order kinetic model (Table 4.5). (2002) (Arslan et al.). The rate expression can replace concentration for absorbance because the Lambert-Beer equation states that the absorbance of a detected molecule is proportional to its concentration. Equation 4.1's slope of the logarithmic plot of absorbance, A vs. treatment time, t, was used to compute the decolorization rate constant, k, on the assumption that the azo dye (methyl orange) decolorization in the Fenton process would follow pseudo-first-order reaction kinetics.

$$\text{Pseudo first order kinetic: } \ln\frac{Ao}{At} = -kdt \quad \text{(Eqn 4.1)}$$

The following equation 4.2 was employed to validate Ho and McKay's (1998) pseudo-second order model. Ae is the equilibrium absorbance of the dye. The estimated pseudo-second order rate constant was obtained from the plot of t=At vs. t. In Table 4.5, the calculated value of k is displayed. The two models' correlation coefficients, R^2 were compared to determine which one best represented the experimental data. Kinetic plots revealed that the rate constants for the pseudo first order model were greater than those for the pseudo second order model. Figures 4.12 and 4.13, respectively, provide plots of the pseudo-first-order and pseudo-second-order kinetic models for the breakdown of the azo dye (methyl orange) using the following equation (Eqn 4.2). Ae is the equilibrium absorbance of the dye. The pseudo second order rate constant was obtained from the plot of t=At versus t. The value of h obtained is presented in Table 4.5. In order to fit the best experimental data, correlation coefficient R^2 of both models were compared. The rate constants obtained from kinetic plots of the pseudo first order model were higher than that of the pseudo second order model. Figure 4.12 and Figure 4.13 shown plots of pseudo first-order and pseudo-second-order kinetic model for the degradation of azo dye (methyl orange) respectively.

Pseudo second order: $\frac{t}{A_t} = \frac{1}{k_2 A_e^2} + \frac{t}{A_e}$ (Eqn 4.2)

The coefficients of correlation of the kinetic study of the pseudo-first order are very close to unity and are more than the pseudo second order values. However, since the pseudo-second order rate values in this investigation also followed a specific trend with a positive kinetic value, as shown in Table 4.5. Arslan and Balcioglu (2021), Giwa et al. (2018), and Abou-Gamra (2013) found negative values for their pseudo second order due

to the absence of a catalyst in their Fenton reaction. The pre-exponential component of the Arrhenius equation is always positive; hence the rate constant can never be negative. The persistence of the negative value for k_2 indicates that the pseudo-second order kinetic model was unable to satisfactorily explain the experimental results. The inclusion of just one reactant theoretically establishes a reaction's pseudo-first order, whereas the involvement of both reactants theoretically establishes a reaction's pseudo-second order. It was proved in this work as the pseudo second order shows positive values. Meaning that the reaction of HEA milled-powder catalyst take part in the Fenton reaction.

Table 4.5 Pseudo first order and pseudo second order of HEA milled powder as catalyst in Fenton process

	PSEUDO FIRST ORDER		PSEUDO SECOND ORDER	
	$k_1\ (min^{-1})$	R^2	$k_2\ (min^{-1})$	R^2
HEA-1	0.1494	0.57411	0.00013	0.40823
HEA-2	0.1537	0.72339	0.104027	-0.31775
HEA-3	0.1312	0.63984	0.234943	-0.24667
HEA-4	0.1414	0.59446	0.087618	0.80163
HEA-5	0.1439	0.65308	0.110301	0.05501
HEA-6	0.1465	0.76702	0.109535	0.47538

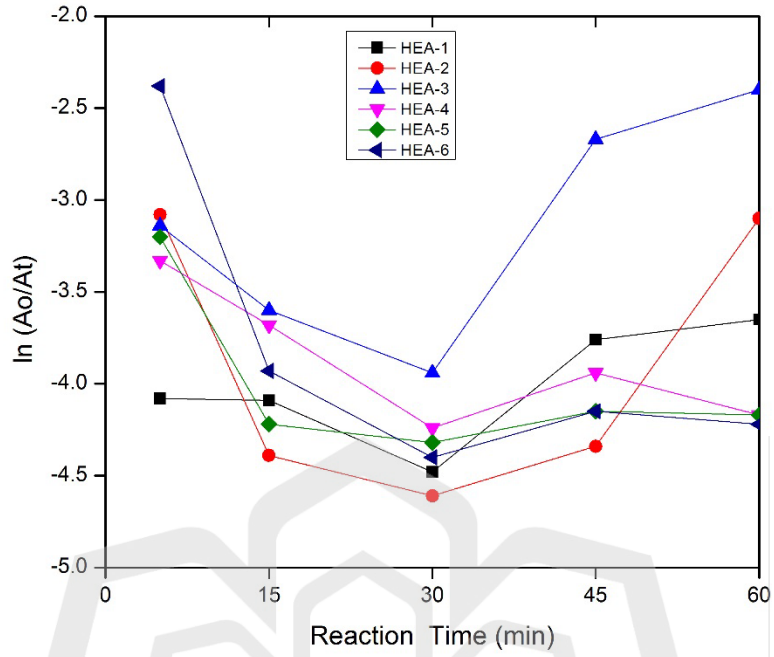

Figure 4.12 Plots of pseudo first-order kinetic model for the degradation of azo dye (methyl orange)

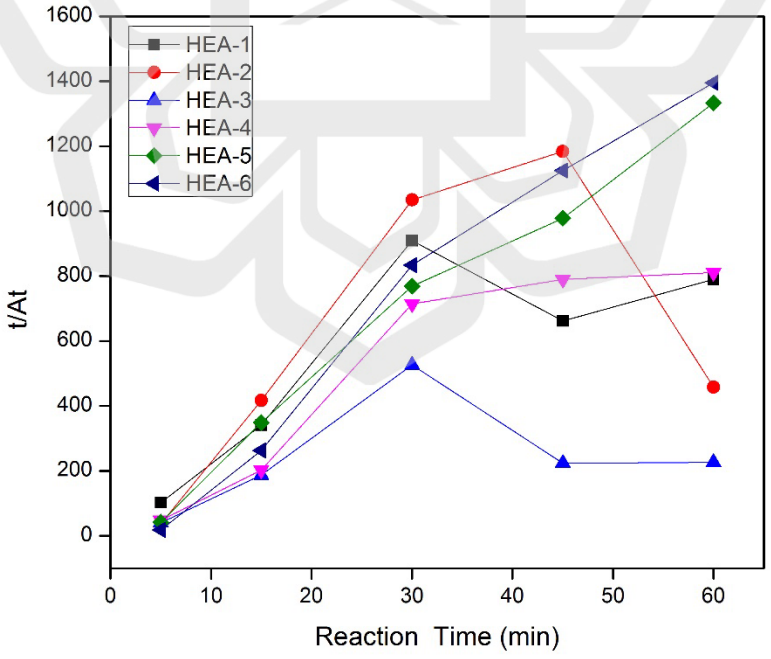

Figure 4.13 Plots of pseudo-second-order kinetic model for the degradation of azo dye (methyl orange)

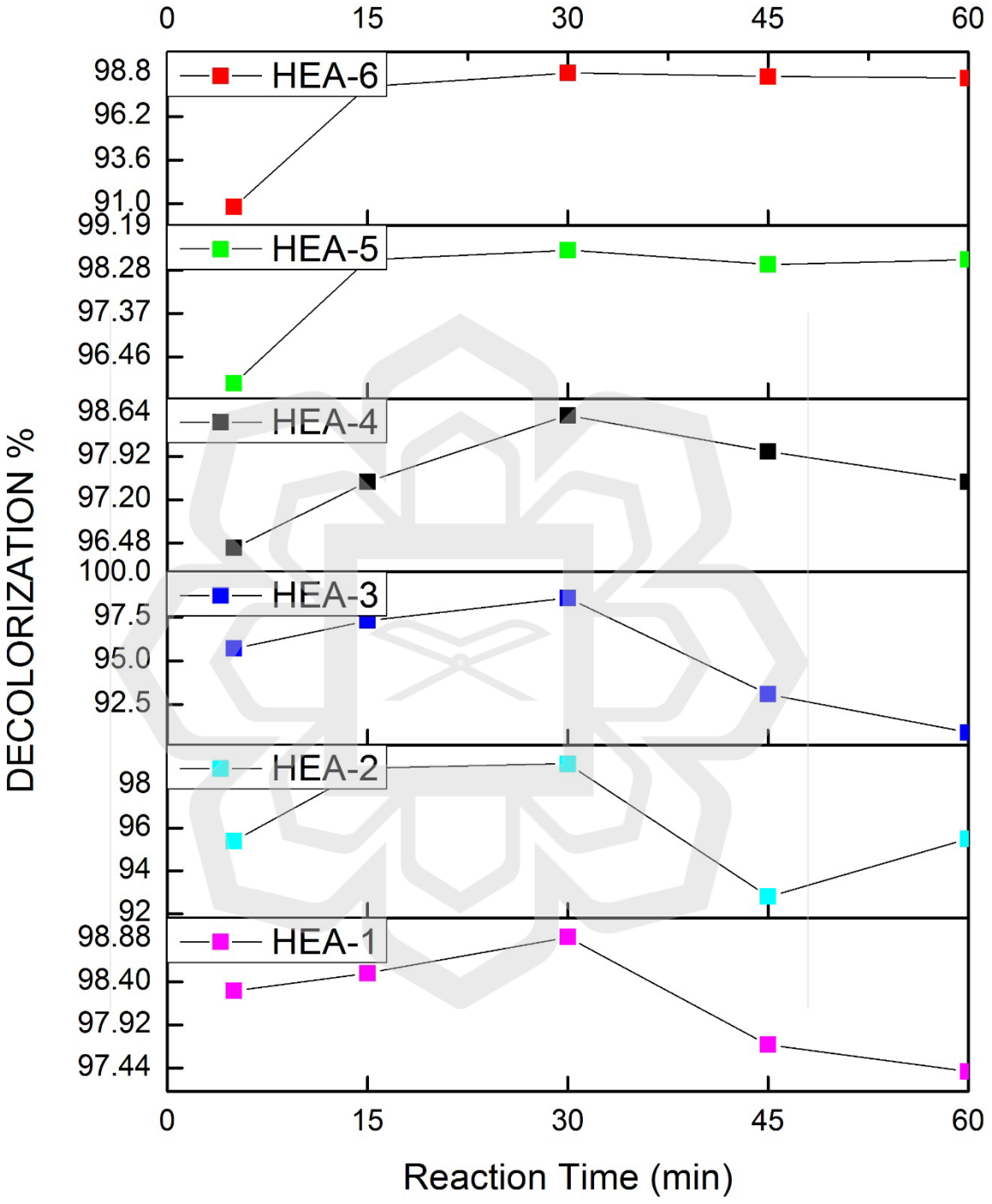

Figure 4.14 Fenton process with different composition of B of HEA catalyst over 60 min reaction time

4.6 Influence of HEA Catalyst to the Kinetics Reaction

According to Table 4.4 the optimum kinetic reactions can be seen in HEA-2 milled-powder with the highest degradation efficiency value. This result is also correlated with the influence of pH value as discussed in section 4.2.2. In addition, the optimum time for the Fenton reaction occurs at 30 minutes over 60 minutes' reaction time as shown in Figure 4.14. It shows that the degradation efficiency of all HEAs are highest at 30 minutes of Fenton reaction. This was proved by the highest K value of pseudo first order and second order at 30 minutes' reaction time (refer Table 4.5). However, the K value decreasing as further increase of reaction time. This is due to the rate of a reaction decreases as time progresses. Theoretically, the theory of collision stated that the rate of reaction depends on the reactant particles colliding with HEA milled-powder active site of the activation energy for the reaction (S.G. Christov, 2012). Meanwhile, the Rate Law specified that reaction rate decreases with time due to the reactants are converted to products (P.Purwanto et al., 2020).

To date, there is still no experimental study on degradation mechanism of HEA catalyst. However, the possible degradation mechanism of azo dye (methyl orange) by HEAs can be illustrated as in Figure 4.15 (L.Ji et al., 2020). The combination of unique crystal structure with severe lattice distortion, residual stress and stored plastic deformation energy of HEAs possess more potential energy and active sites which are responsible for excellent degradation capacity of HEAs powder toward an azo dye (methyl orange). Next, the reduction behavior of hydrogen ([H]) plays a role as a reduction agent to reduce various organic species. The [H] can induce the cleavage of azo bonds and destroy the chromophore groups because [H] exhibits high reactivity. The hydrogen ([H]) is formed when a large number of electrons are released by HEAs and combine with hydrogen ions in water. Thus,

HEAs as catalyst in Fenton process will enhance the degradation performance of azo dye (methyl orange) by promoting high surface area and active sites to increase the formation hydroxyl radical during the Fenton process in order to break the azo bond and decolorized the azo dye (methyl orange) effluents. The reactions of the above discussion were described as in equation 4.3, 4.4 and 4.5 where M is metal, ne is number of electron, H2O is water, H+ is hydrogen ion, OH- is hydroxide, R is radical and NH2 is amine group from azo dye (methyl orange).

$$M \rightarrow M^{+} + ne^{-} \quad \text{(Eqn. 4.3)}$$

$$H_2O \rightarrow H^{+} + OH^{-} \quad \text{(Eqn. 4.4)}$$

$$R - N = N - R_1 \; + 4H^{+} + 4e^{-} \rightarrow R - NH_2 + R_1 - NH_2 \quad \text{(Eqn. 4.5)}$$

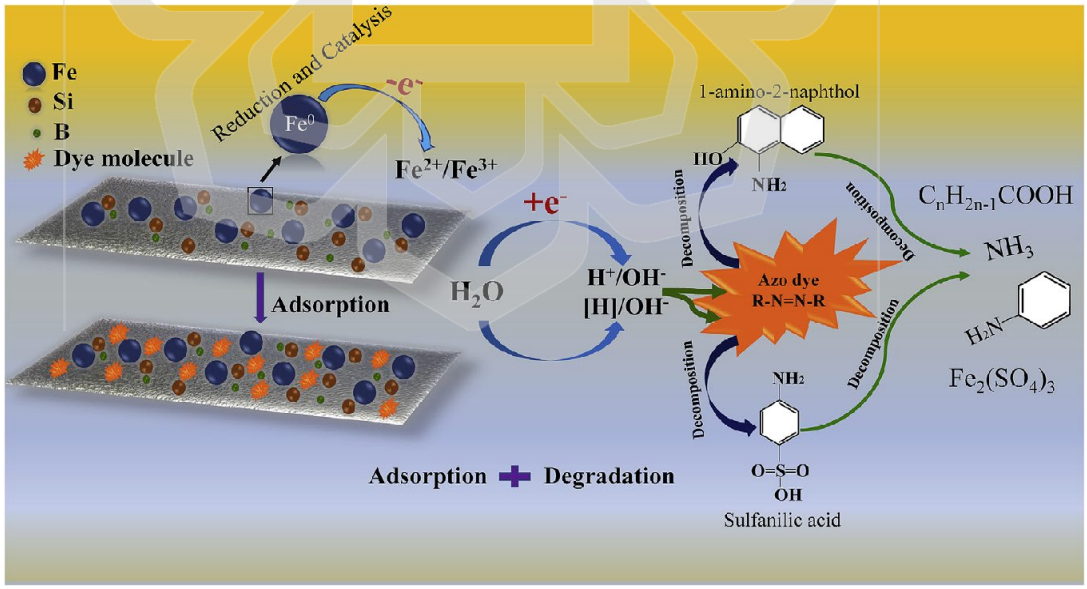

Figure 4.15 Possible degradation mechanism of HEA as catalyst (Lv et al., 2016)

Therefore, it can be concluded that, the presence of HEA as catalyst could enhance the performance of dye degradation in Fenton process. This will speed up the process and reduce the formation of sludge.

4.7 Summary

This chapter presents results and the discussion of the development of the HEA powders, the effect of the Fenton process with different ratios of Fenton reagent, the effect of degradation efficiency of azo dye with different boron compositions and an analysis of the catalytic mechanism of HEA milled powder in the Fenton process. According to the results, the HEA powder was successfully produced with 0.94μm particle size at 160 hours milling time with the good homogeneity using ball milling method. Different ratio of Fenton reagent was manipulated to obtain the optimum parameters ratio. The optimum ratio of the Fenton reagent was used to determine the effect of HEA powder as a catalyst. Fenton reagents with a Fe^{2+}/H_2O_2 molar ratio of 10:1 have the best degradation efficiency (96%). The degradation of azo dye with HEA powder as catalyst was then performed. The effect of boron composition in the HEA powder was investigated and it was showed that HEA-2 showed 99 % degradation efficiency at 30 minutes over one hour during Fenton. The kinetics mechanism was also determined by pseudo first and second order reaction which shows that HEA-2 has highest activation energy among the other compositions of B in HEAs. These findings show that the HEA powder is a good potential material as catalyst to improve Fenton process.

CHAPTER FIVE

CONCLUSIONS AND RECOMMENDATIONS

5.1 Conclusions

Development of HEA powder by planetary ball milling process is achieved. Three phases of crystal structure which are FCC, BCC and BCC/B2 are present in HEA-1, HEA-2 and HEA-3 with the addition of intermetallic boride Fe2B indicates the presence of B. This shows that all the elements in HEA are diffused completely to become HEA. The particle size of HEA powder reduces over milling time as 0.960µm, 1.167µm, 1.344µm, 2.00µm and 0.943µm at 5H, 30H, 70H, 100H and 160H respectively. Reduction of particle sizes during the milling process will exhibit high surface area and more active catalytic sites of HEA. The optimum ratio of $[Fe^{2+}]$ / $[H_2O_2]$ was found to give the best result for the decolorization of azo dye (methyl orange) in the Fenton process. Fenton reagents with a Fe2+/H2O2 molar ratio of 10:1 have the best degradation efficiency (99%) at 1 hour over 2 hours of Fenton reaction. Furthermore, the presence of B in HEA improves the Fenton reaction by attracting additional acid sites. This may be shown in the Fenton process, where best degradation efficiency of azo dye (methyl orange) was found at HEA-2 with composition 0.02 wt% of B which is 99.8 % at 30 minutes over one hour of Fenton reaction. The kinetic reaction of as catalyst in Fenton reaction was also determined by pseudo first and second order reaction which shows that HEA-2 has the highest activation energy among the other compositions of B in HEAs.

5.2 Recommendations

1. To study the amount of sludge produced with the presence of HEA and without HEA as catalyst.
2. To study the effect of temperature on degradation efficiency of HEA in degrading azo dye (methyl orange).
3. To run the Fenton reaction with HEA as catalyst on wastewater from the textile industry.

REFERENCES

Akira, T., & Akihisa, I. (2005). Classification of Bulk Metallic Glasses by Atomic Size Difference, Heat of Mixing and Period of Constituent Elements and Its Application to Characterization of the Main Alloying Element. Materials Transactions, 46 (12), 2817-2829.

Abu Hassan, N., Zin, N., Shaari, N., Fadil, N., Jami, M., & Nordin, N. (2022). Characterizations of High Entropy Alloy Powder as Catalyst Synthesized by Mechanical Alloying for Azo Dye Degradation. Key Engineering Materials, 908, 419-425.

Alfaya, E., Iglesias, O., Pazos, M., & Sanromán, M. (2015). Environmental application of an industrial waste as catalyst for the electro-Fenton-like treatment of organic pollutants. RSC Advances, 5(19), 14416-14424.

Cantor, B., Chang, I.T.H., Knight, P. & Vincent, A.J.B. (2004). Microstructural Development in Equiatomic Multicomponent Alloys. Materials Science and Engineering, 375–377, 213-218,

Bello, M., & Raman, A. (2018). Synergy of adsorption and advanced oxidation processes in recalcitrant wastewater treatment. Environmental Chemistry Letters, 17(2), 1125-1142.

Brüschweiler, B., & Merlot, C. (2017). Azo dyes in clothing textiles can be cleaved into a series of mutagenic aromatic amines which are not regulated yet. Regulatory Toxicology and Pharmacology, 88, 214-226.

Burrows, H., Canle L, M., Santaballa, J., & Steenken, S. (2002). Reaction pathways and mechanisms of photodegradation of pesticides. Journal of Photochemistry and Photobiology B: Biology, 67(2), 71-108.

Burbano, A., Dionysiou, D., Suidan, M., Richardson, T. (2003). Chemical destruction of MTBE using Fenton's Reagent: Effect of ferrous iron/hydrogen peroxide ratio. Water Science and Technology: A Journal of the International Association on Water Pollution Research, 47.

Cui, X., Zhang, B., Zeng, C., & Guo, S. (2018). Electrocatalytic activity of high-entropy alloys toward oxygen evolution reaction. MRS Communications, 8(3), 1230-1235.

Da Cruz Severo, E., Dotto, G., Silvestri, S., dos Santos Nunes, I., da Silveira Salla, J., & Martinez de la Cruz, A. et al. (2020). Improved catalytic activity of EDTA modified BiFeO3 powders for remarkable degradation of procion red by heterogeneous photo–Fenton process. Journal of Environmental Chemical Engineering, 8(4), 103853.

Dehghani, M., Shahsavani, E., Farzadkia, M., & Samaei, M. (2014). Optimizing Photo Fenton like process for the removal of diesel fuel from the aqueous phase. Journal of Environmental Health Science and Engineering, 12(1).

Ellen MacArthur Foundation (2017). A New Textile Economy: Redesigning Fashion's Future. Retrieved on December 8, 2020 from

Giwa, A. A., Bello, I. A., Olabintan, A. B., Bello, O. S., & Saleh, T. A. (2020). Kinetic and thermodynamic studies of fenton oxidative decolorization of methylene blue. Heliyon, 6(8), e04454.

Gordon, P., & Gregory, P. (1983). Organic Chemistry in Colour (pp. 57-66). Springer Verlag Berlin Heidelberg 1987.

Hassan, N., Natsir, N., Rahman, S., Daud, F., Jamal, N., Ibrahim, N., & Nordin, N. (2021). Development of High Entropy Alloy (HEA) as Catalyst for Azo Dye Degradation in Fenton Process. Journal of Physics: Conference Series, 2129(1), 012101.

Hussain, S., Aneggi, E. & Goi, D. (2021). Catalytic activity of metals in heterogeneous Fenton-like oxidation of wastewater contaminants: a review. Environmental Chemistry Letters, 19(3), 2405–2424.

Jamee, R., & Siddique, R. (2019). Biodegradation of Synthetic Dyes of Textile Effluent by Microorganisms: An Environmentally and Economically Sustainable Approach. European journal of microbiology & immunology, 9(4), 114–118.

Kaur, P., Sangal, V.K., & Kushwaha, J.P. (2018). Parametric study of electro-Fenton treatment for real textile wastewater, disposal study and its cost analysis. International Journal of Environmental Science and Technology, 16, 801-810.

Lv, Z. Y., Liu, X. J., Jia, B., Wang, H., Wu, Y., & Lu, Z. P. (2016). Development of a novel high entropy alloy with eminent efficiency of degrading azo dye solutions. Scientific reports, 6, 34213.

Matyszczak, G., Sędkowska, A., & Kuś, S. (2020). Comparative degradation of Metanil Yellowin the electro-Fenton process with different catalysts: A simplified kinetic model study. Dyes and Pigments, 174, 1–6.

Matyszczak, G., Krzyczkowska, K., & Fidler, A. (2020). A novel, two electron catalysts for the electro-Fenton process. Journal of Water Process Engineering, 36, 101242.

Mingqing, Z., Seonghoon, Y., & Junhyeok, C. (2021). Excellent dye degradation performance of FeSiBP amorphous alloys by Fenton-like process. Journal of Environmental Sciences,105, 116-127.

Miracle, D. B. (2019). High entropy alloys as a bold step forward in alloy development. Nature Communications, 10(1), 1805.

Moravcik, I., Kubicek, A., Moravcikova-Gouvea, L., Adam, O., Kana, V., Pouchly, V., Zadera, A., & Dlouhy, I. (2020). The Origins of High-Entropy Alloy Contamination Induced by Mechanical Alloying and Sintering. Metals - Open Access Metallurgy Journal.

Muhammad, A., & Mashi, A. (2020). Application of Central Composite Design to the Photo Fenton Degradation of Methyl Orange Azo Dye Using Fe-Activated Carbon Catalyst.Volume 5 - 2020, Issue 8 - August, 5(8), 479-485.

Nordin, N., Zhaoyuan, L., Goodall, R., & Todd, I. (2022). Theoretical critical metastability temperature to interpret phase formation in a lamellar-like-structured high entropy alloy. Journal of Materials Research and Technology, 18, 2519-2530.

Ning, W. (2022). FeCoNiMnCuTi high entropy amorphous alloys and M50Ti50 (M = Fe, Cu, FeCoNiMnCu) amorphous alloys: Novel and efficient catalysts for heterogeneous photo-Fenton decomposition of Rhodamine B. Surfaces and Interfaces, Volume 33, 102265.

Pang, Y., & Abdullah, A. (2013). Current Status of Textile Industry Wastewater Management and Research Progress in Malaysia: A Review. CLEAN - Soil, Air, Water, 41(8), 751-764.

P.V. Nidheesh & R. Gandhimathi (2012). Trends in electro-Fenton process for water and wastewater treatment: An overview. Desalination, 299.

Ragimiri (2006). A typical azo compound: 4-hydroxyphenylazobenzene aka yellow azo dye (methyl orange). Retrieved on August, 2021 from www.wikidoc.org.

Ramírez, J., Castillo, P., Ceden˜o, L., Cuevas, R., Castillo, M.A., Palacios, J.M., & López, A. (1995). Effect of boron addition on the activity and selectivity of hydrotreating CoMo/Al2O3 catalysts. Applied Catalysis A-general, 132, 317-334.

Sabhi, S., & Kiwi, J. (2001). Degradation of 2,4-dichlorophenol by immobilized iron catalysts. Water research, 35 8, 1994-2002.

Shivam, V., Basu, J., Pandey, V. K., Shadangi, Y., & Mukhopadhyay, N. K. (2018) Alloying behaviour, thermal stability and phase evolution in quinary AlCoCrFeNi high entropy alloy. Advanced Powder Technology, 29(9), 2221–223.

Tsai, M. H., & Yeh, J. W. (2014). High-entropy alloys: a critical review. Materials Research Letters, 2(3), 107-123.

United Nations Environment Programme (UNEP) (2018, November 12). Putting The Brakes on Fast Fashion. Retrieved on December 8, 2020 from www.unep.org.

Wang, S., & Xin, H. (2019). Predicting Catalytic Activity of High-Entropy Alloys for Electrocatalysis. Chem, 5(3), 502–504.

Wang, N., Zheng, T., Zhang, G., & Wang, P. (2016). A review on Fenton-like processes for organic wastewater treatment. Journal of Environmental Chemical Engineering, 4(1), 762–787.

Wang, C., & Shih, Y. (2015). Degradation and detoxification of diazinon by sono-Fenton and sono-Fenton-like processes. Separation and Purification Technology, 140, 6 12.

Wang, H., Wei, R., Li, X., Ma, X., Hao, X., & Guan, G. (2020). Nanostructured amorphous Fe29Co27Ni23Si9B12 high-entropy-alloy: an efficient electrocatalyst for oxygen evolution reaction. Journal of Materials Science & Technology.

Wei, R., Zhang, K., Zhao, P., An, Y., Tang, C., Chen, C., & Hao, X. (2021). Defect-rich FeCoNiPB/(FeCoNi)3O4-x high-entropy composite nanoparticles for oxygen evolution reaction: Impact of surface activation. Applied Surface Science, 549, 149327.

Wu, S., Pan, Y., Wang, N., Dai, W., Lu, J., & Lu, T. (2018). Rapid decoloration of azo dye Direct Blue 6 by AlCrFeMn high entropy alloy. RSC Advances, 8(72), 41347 41354.

Wu S., Pan Y., Wang N., Lu T., & Dai W. (2019). Azo dye (methyl orange) degradation behavior of AlFeMnTiM (M = Cr, Co, Ni) high-entropy alloys. International Journal of Minerals Metallurgy, and Materials, 26, 124-132.

Yang, C., Wang, D., & Tag, Q. (2014). The synthesis of NdFeB magnetic activated carbon and its application in degradation of azo dye (methyl orange) methyl orange by Fenton-like process. Journal of the Taiwan Institute of Chemical Engineers, 45(5), 2584–2589.

Xu, M., Wu, C., & Zhou, Y. (2020). Advancements in the Fenton Process for Wastewater Treatment. In (Ed.), Advanced Oxidation Processes - Applications, Trends, and Prospects. IntechOpen.

Yeh, J. (2006). Recent Progress in High-entropy Alloys. European Journal of Control, 31(6), 633-648.

Yu, Y., Liu, W. M., Zhang, T. B., Li, J. S., Wang, J., Kou, H. C., & Li, J. (2013). Microstructureand Tribological Properties of AlCoCrFeNiTi0.5 High-Entropy Alloy in Hydrogen Peroxide Solution. Metallurgical and Materials Transactions, 45(1), 201–207.

Yuan, S., Gou, N., Alshawabkeh, A.N., & Gu, A.Z. (2013). Efficient degradation of contaminants of emerging concerns by a new electro-Fenton process with Ti/MMO cathode.Chemosphere, 93 11, 2796-804.

Zhang, M. H., Dong, H., Zhao, L., Wang, D. X., & Meng, D. (2019). A review on Fenton processfor organic wastewater treatment based on optimization perspective. The Science of the total environment, 670, 110–121.

Zhang, K. B., Fu, Z. Y., Zhang, J. Y., Shi, J., Wang, W. M., Wang, H., & Zhang, Q. J. (2009). Nanocrystalline CoCrFeNiCuAl high-entropy solid solution synthesized by mechanical alloying. Journal of Alloys and Compounds, 485, 1-2.

APPENDIX 1

DR NORHUDA HIDAYAH NORDIN
Assistant Professor
Department of Manufacturing and Materials Engineering
Kulliyyah of Engineering
International Islamic University Malaysia

LIST OF PUBLICATION PAPER

1. **Title: <u>Development of High Entropy Alloy (HEA) as Catalyst for Azo Dye Degradation in Fenton Process</u>**
   - Hyperlink: https://iopscience.iop.org/article/10.1088/1742-6596/2129/1/012101
   - DOI: 10.1088/1742-6596/2129/1/012101
   - Published Online: December 2021
   - Published in Archives of Metallurgy and Materials, number 1/2023, volume 68.

2. **Title: <u>Characterizations of High Entropy Alloy Powder as Catalyst Synthesized by Mechanical Alloying for Azo Dye Degradation</u>**
   - Hyperlink: https://www.scientific.net/KEM.908.419
   - DOI: https://doi.org/10.4028/p-25ajxn
   - Published Online: January 2022

3. **Title: <u>High entropy alloy as catalyst for degradation of azo dye in Fenton process</u>**
   - Hyperlink: https://aip.scitation.org/doi/abs/10.1063/5.0079480
   - DOI: https://doi.org/10.1063/5.0079480
   - Published Online: June 2022

4. **Title: <u>Enhancement of Fenton Process using High Entropy Alloy (HEA) Powder as Catalyst</u>**

   - This title was presented during International Conference of Advance Manufacturing and Materials ICAMME, IIUM on August 2022
   - This article \published in Lecturer Notes of Mechanical Engineering journal.

DR NORHUDA HIDAYAH NORDIN
Assistant Professor
Department of Manufacturing and Materials Engineering
Kulliyyah of Engineering
International Islamic University Malaysia